FLEXURAL FATIGUE BEHAVIOUR OF KEVLAR FABRIC REINFORCED EPOXY RESIN COMPOSITES

A Thesis Submitted
In Partial Fulfilment of the Requirements
for the Degree of
MASTER OF TECHNOLOGY

by
BHARAT BHUSHAN

to the
DEPARTMENT OF MECHANICAL ENGINEERING
INDIAN INSTITUTE OF TECHNOLOGY, KANPUR

APRIL, 1987

CERTIFICATE

This is to certify that the thesis entitled, "FLEXURAL FATIGUE BEHAVIOUR OF KEVLAR FABRIC REINFORCED EPOXY RESIN COMPOSITES," by Bharat Bhushan is a record of the work carried out under my supervision and has not been submitted elsewhere for a degree.

(B. D. Agarwal)
Professor
Mechanical Engineering Department
Indian Institute of Technology
Kanpur 208 016

March, 1987

ACKNOWLEDGEMENTS

I wish to express my deep sense of gratitude and appreciation to thesis advisor, Prof. B.D. Agarwal for his valuable guidance throughout the present work. His generous attitude towards academic liberty has been a constant source of inspiration for me.

I am grateful to Prof. Prashant Kumar for his valuable suggestions and helps.

I deeply appreciate the discussions and helpful commen of my friends Dinesh Shukla and K.K. Bajpai. I highly value the association with my friends G.K. Adil, Sanjeev Gupta, G.K. Tripathy, R.J.S. Bagga and others with whom I shared my ideas.

Thanks are due to Messrs S.L. Srivastava, D.K. Sarkar, Swaran Singh, Duvedy, B.D. Pandey, P.N. Pandey and Avinash of the Mechanical Engineering Department for their help.

I wish to thank Swami Anand Chaitanya for the excellen typing of the manuscript and Mr. B.K. Jain for the neat tracings.

Bharat Bhushan

March, 1987

CONTENTS

LIST OF FIGURES

ABSTRACT

Investigations have been carried out on Kevlar fabric reinforced epoxy resin fabricated in the laboratory by hand layup technique. The flexural fatigue tests were performed on flat specimens in cantilever bending under stroke controlled mode with zero mean deflection. A fatigue testing machine available in laboratory is modified and used for the testing. The degradation in fatigue secant modulus i.e. the modulus at maximum strain point, has been taken as a measure of internal damage in specimen. To measure the fatigue secant modulus maximum bending moment at the fixed end of the specimen was measured by the means of a dynamometer. The failure of the specimen was defined by a secant modulus failure criterion i.e. failure occurs when the fatigue secant modulus reduces to static secant modulus.

It was found that, although, the damage accumulation depends on applied stress level, it follows a definite trend. The damage accumulation can be divided into three steps, the damage initiation, steady damage, and the damage propagation. A damage model has been proposed to predict the damage accumulation with the number of fatigue cycles. It consists of a strain dependent monotonically increasing damage rate term and

another strain dependent monotonically decreasing damage rate term moderated by a strain dependent weighing parameter. The S-N curve has been defined by a linear law between normalized fatigue stress or strain and log of fatigue life as well as by a power law between normalized fatigue stress or strain and fatigue life. The scatter in fatigue life data has been analysed by a two parameter Weibull distribution and probability S-N curves have been drawn.

CHAPTER 1

INTRODUCTION

1.1 COMPOSITE MATERIALS:

A material made by the combination of two or more macroconstituents differing in form and/or material composition and that are essentially insoluble in each other is called a composite material.

Fibre reinforced composites are relatively new materials but they have already become important engineering materials. They are well known for their light weight, high strength, high stiffness and controlled anisotropic properties. Additional advantage that composits offer over the conventional materials include flexibility in design, ease of fabrication, corrosion resistance, etc. Today, fibre composites have found such diverse applications as space vehicles, aircraft, offshore structures, automobiles, protective armours, containers, corrosion resistance coatings, sporting goods, electronics and appliances.

Now a days the most widely used fibrous composites are glass-, graphite-, Kevlar - and boron- fibre composites. E- glass fibre composites are most developed and widely used because of its relative low cost. It has a very high tensile strength, but low stiffness. Boron, graphite, and Kevlar (as

compared to glass) fibres are most exceptional because of their high stiffness values, although they are costlier. Of these, the graphite fibres offer a large variety with different combinations of modulus and strength values. It has high compression strength and a moderate density. It is used in stiffness critical and compression critical uses and the uses where high specific modulus is required. Boron fibres has highest modulus and strength, but also high density. Because of its better high temperature properties it is used in high temperature uses; as in aircrafts etc. Because of its highest strength, lowest density and low cost as compared to graphite and boron fibre, Kevlar fibres have become an important reinforcement material today. It has various other favourable qualities. The importance of the Kevlar fibre composites are increasing continuously in practical uses. Kevlar fibre reinforced composites is the subject of present investigations.

Kevlar Fibre Composites:

Introduced commercially in the early seventies, Kevlar aramid fibre is an aromatic polyamide fibre. It is an aromatic organic compound of carbon, hydrogen, oxygen and nitrogen. Excellent properties of the Kevlar fibre composites are low density, high tensile strength, moderate tensile modulus, high fracture toughness, and high impact resistance. Some additional properties are chemical and mechanical stability over a wide range of temperature (-196 to 204°C depending upon resin),

corrosion resistance, electrical non-conductivity etc. But it has low compressive properties as a result of poor coupling property of fibre with resin matrix. Also the moisture absorption by the fibres is high.

Kevlar fibre composites are used in tension critical structures, ballistic protections and indifferent high performance composite applications. The wide application of Kevlar fibre composites include the use in rocket engine cases, airplanes components, helicopter blade and other parts, boats, snowmobiles, tracks, offshore structure, pressure vessels, conveyors, ropes and cables, sporting goods as golf stick etc, helmets, protective gloves, ballistic protective vests etc.

In service, almost all the above mentioned components experience the repeated loading and vibrations. Which necessiates the fatigue analysis of material. The lack of data available for Kevlar in fatigue, results in selection of its fatigue testing for present investigation.

1.2 FATIGUE OF COMPOSITES:

Composite materials are being used in a variety of structures that must not fail. However, it has been learnt from experience that nothing lasts forever and every structure or component built possesses a finite service life. Unexpected or premature failures often carry economic or safety implications and must be avoided. It is, therefore, imperative that a

method exists to provide an estimate of the life time under service conditions, that makes fatigue analysis an important consideration.

Two important features of the fatigue of composites as compared to that of metals are that composites exhibit evidence of physical damage to the material much before the final fracture whereas metals exhibit cracks just prior to final fracture. Secondly, microevents which reduce the strength and stiffness, and determine the life of composites are complex, various and intricately connected to a variety of failure modes under different circumstances whereas metal exhibit one failure mode cracking. Failure modes for composite includes fibre breakage, delamination, matrix cracking, interface debonding, void growth and/or combination of them.

Composites have been shown to be more sensitive to strain range as compared to metal [1]. This results in the high cycle fatigue strength of composites being high with respect to static and low cycle fatigue strength. That is, fatigue damage for composites is more critical in low cycle fatigue region than high cycle fatigue region, whereas for metal fatigue damage may critical for high cycle fatigue.

Although the tensile strength of unidirectional composites is a maximum at a direction of 0° to the fibres, in fatigue the unidirectional construction is not optimum [1]. The best explanation for this phenomenon is the fact that unidirectional material is subjected to splitting and rapid crack propagation

in the matrix parallel to the fibre. In general, unwoven materials are superior to woven materials in fatigue because fibres in unwoven materials are straight and parallel and do not get crimped as in the woven fabric construction [2].

High modulus fibre reinforced composites, such as Kevlar-, born-, and graphite- reinforced polymers, display excellent fatigue resistance when tested in directions in which the properties are fibre controlled. In general, it can be stated that the excellent fatigue resistance of these materials results from the environmental stability of the high modulus fibres and their low strains to failure, which, as a result, produces low strains in the matrix.

A limited work has been conducted on the fatigue behaviour of Kevlar-49/ epoxy composites. Limited fatigue data supplied by the fibre manufacturer and Minar et.al.[3] (Fig.1.1), shows the fatigue behaviour of Kevlar-49/epoxy. Comparison of fatigue behaviour shows that Kevlar-49/epoxy exhibits comparable fatigue properties to born/epoxy and graphite/epoxy. Kevlar-49/epoxy displays far superior fatigue properties compared to glass-epoxy and aluminium. Hanstad [4] has worked on Kevlar-49/epoxy strands. He found the fatigue life varied from approximately 2000-76000 cycles for a simusoidal loads varying from 1- 88 % of strand failure strength at 10 Hz. These results shows a large scatter in fatigue life data. Bunsell [5] working on Kevlar-49 fibre found that Kevlar-49 is

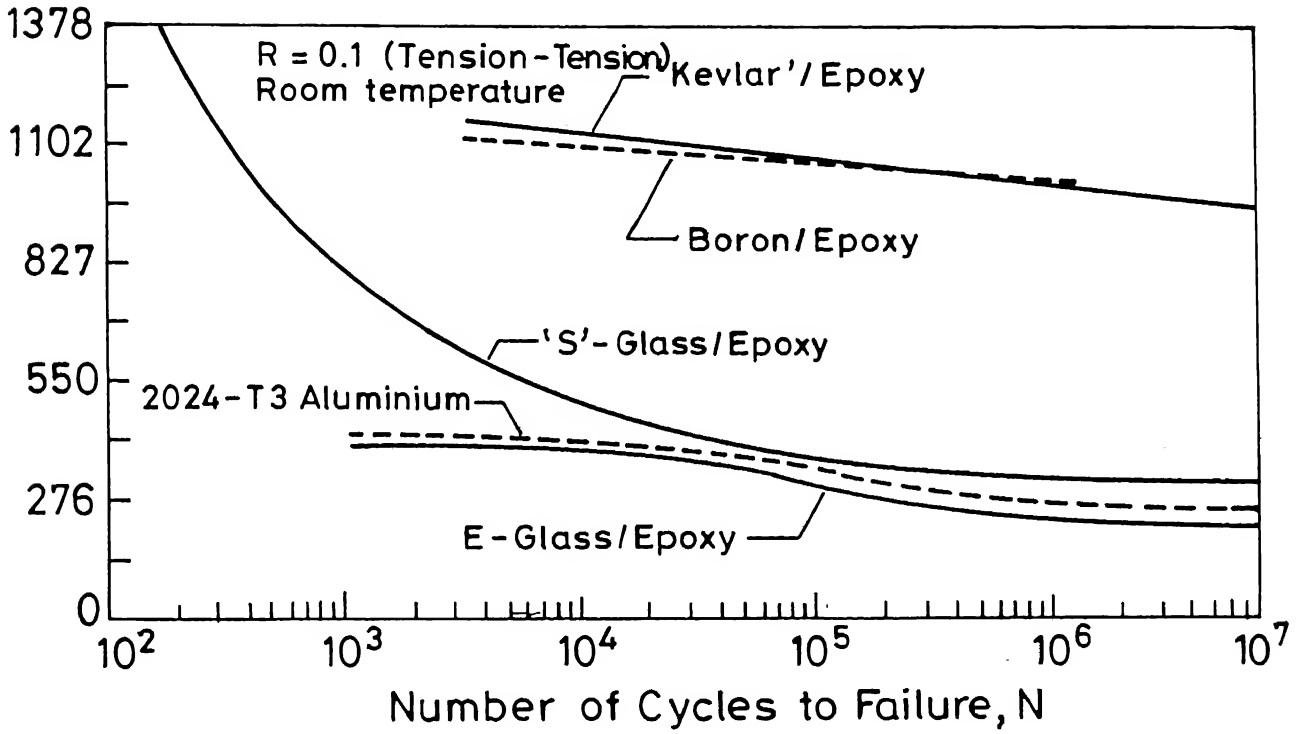

Fig. 1.1 Comparison of fatigue characteristics of some unidirectional composites and aluminium.

considered to have high resistance to fatigue damage as compared to other polymeric fibres. Kevlar does not heat-up significantly during fatigue. The effect of stress range at constant maximum load is significant for Kevlar composites.

1.3 LITERATURE SURVEY:

Fatigue of composites has been extensively studied. However, a very few studies [3] appear to have been conducted on fatigue of Kevlar fiber composite materials. The fatigue of glass fiber composite material has been explored extensively[6-21]. A lot of work has been done on carbon [12,13,17,22-24] and boron[25 fiber composites too. Although, flexural fatigue testing is more common for metals because of their isotropic properties, for composites more work have been done in axial fatigue [6-14,17, 22-24,26]. However, flexural fatigue is also studied by many investigators [15-21].

In general fatigue properties of composites are influenced by various material and testing variables such as, (1) matrix material, (2) volume fraction of reinforcement, (3) ply orientation and stacking sequence, (4) type of weave, (5) interface properties, (6) type of loading, (7) mean and alternating stresses, (8) cyclic frequency and (9) environmental conditions, etc.

Boller [27] and Davis et.al. [28] have evaluated a variety of matrix system and found epoxy to be superior in fatigue. Many investigators [9,27-30] have studied the effect of fiber content on fatigue properties of composites. They found fatigue strength

is higher for higher fiber contents but beyond an optimum point strength decreases. The effect of fiber orientation is complex and it is found that unidirectional construction is not optimum [1]. The stacking sequence also influences the fatigue life, mainly for flexural fatigue. Davis et.al.[28] have given the S-N curves for various types of nonwoven and woven fabric for both axial and flexural fatigue. Dally and Agarwal [7,8] suggested that either of strain or stress controlled fatigue tests can be used in low cycle fatigue studies. Kim and Ebert [21] tried various control mode and found load control as most damaging and stroke control as least damaging whereas damage mode is unaffected by control mode. Effect of specimen geometry on the strength of composite material have been described by Kaminski [31]. Effect of mean and alternating stresses are shown by Owen et.al. [6] with the help of a master diagram. Salkind [1] found that in fatigue, composites are more sensitive to strain range as compared to metals. The effect of cyclic frequency is less pronounced in metals whereas it is significant for composites [14]. This effect is higher for low cycle fatigue lives than for high cycle fatigue lives [15]. The effect of cyclic frequency is investigated by many others [11,17,21,32] too.

Shih and Ebert [33] have described the different failure modes (tensile, compressive and shear modes) and mechanism in static flexural (4-point bending) tests. Browning et.al. [34] have given a modified beam theory to calculate flexural strength.

They found that discontinuities in the inplane stresses at layer interfaces lead to a state of stress which is difficult to compare to standard laminate tensile coupons. For unidirectional composites they found flexural strength higher than tensile strength because of statistical nature of failure process. Dharan [17] has studied the fatigue behaviour of graphite/polyster composite in completely reversed bending. Agarwal and Joneja [19,20] and Joneja [18] have done a extensive work on flexural fatigue of GFRP in cantilever loading under displacement control mode with zero mean displacement. Similar work had been done by James et.al. [15]. Kim and Ebert [21] have studied the flexural fatigue performance characteristics of unidirectional fiber-glass composites varying the span to thickness ratio in four point bending.

The character and extent of internal damage have been studied by investigators using different methods. Most of the investigators have used change in structural properties such as static or dynamic modulus [7,10,14,17-20,35], residual strength [9,18-20,30], or load decay [16,21] as a measure of internal damage. Hahn and Kim [11] extended the secant modulus degradation criterion as a measure of damage from static to dynamic case.

The failure of the specimens has been defined by different investigators by different failure criterion. Salkind [1] has suggested that fatigue test data be reported in terms of cycles

to a given change in stiffness rather than cycles to fracture. Many investigators [6,18-20] were taken the complete separation as the criterion of failure, whereas few of them and some others [17-20] were considered a loss of known percentage in stiffness as failure. Brogdon [12] used Tsai-Hill failure criterion for fatigue tests. Hahn and Kim [11] first stated that failure occurs when the fatigue secant modulus reduces to within the range of the static secant modulus. O'Brien et.al. [25] defined a secant modulus failure criterion based on the statement of Hahn and Kim [11]. Hwang and Han [35] have given a strain failure criterion.

A large number of investigators have done the fractographic study to find out the damage mechanism. James et.al.[15] have studied the effect of convolution of threads in weaved cloth reinforced plastics. Owen et.al. [6] have distinguished the debonding, cracking and separation phases in fracture of GRP. Damage mechanism for graphite/polyster in flexural fatigue has been studied by Dharan [17]. Mechanism of damage propagation in weaved cloth laminate of GRP is described by Tanimoto et.al. [9]. Kim and Ebert [26] have described the failure sequence and mechanism in axial fatigue of GFRP, later they [14] found that the extent and mode of damage is affected by means and alternating stresses both. They, in their other investigations [21] found that the bending fatigue failure mode of unidirectional fiber-glass composites changes from shear failure

to flexural failure passing a combined failure region as the span to thickness ratio value increases. They described the damage mode for all the three cases by dividing that in four steps.

A lot of investigators have studied the progressive nature of the damage in fatigue of composites. Some of them [9, 18-20,21] studied it qualitatively whereas many others [7,22,24, 36-38] studied it quantitatively and developed the different damage models to predict damage accumulation during fatigue. Dally and Agarwal [7,8] have described that fatigue modulus varied linearly with logarithm of number of cycles. Yang and Jones [22] have proposed a three parameter fatigue and residual strength degradation model to predict statistically the fatigue behaviour of composite laminate under axial shear loading. The fatigue behaviour includes the fatigue life and the fatigue damage expressed in terms of the residual strength degradation. The different statistical strength degradation models have been given by investigators [24,36]. Poursartip et.al. [37] have suggested a general function to described damage accumulation. They have also given three simple examples of the function. Hwang and Han [38] have critically reviewed the available damage models. They have also proposed few new models.

A number of analytical models have been developed by investigators to predict the fatigue life associated with applied stress. Dally and Agarwal [7] had tried several

relationship between applied stress level and different powers of logarithm of fatigue life and found the linear relationship as the best [8, 11]. A power law has been applied by many investigators [10,11]. Several other relationships have been also developed by investigators. Sims et.al. [12] have given a model including oscillatory to mean stress ratio term too. Hahn [36] has given two statistical life prediction models. Sendecky$ [47] has presented a new procedure for getting fatigue models, consisting of a deterministic equation (to find out equivalent static strength to fatigue data) defining the shape of S-N curve and a probabilistic description of data scatter. A new method to predict fatigue life under strain failure criterion has been developed by Hwang and Han [35].

Scatter in the fatigue life data has been analysed by investigators [14,15]. The data scatter has been represented by many distributions such as log normal [6, 14] and Weibull [11, 12,23,24,36,38] distributions. Many investigators [23] analysed the fatigue life separately by distributions whereas some other [22,24] developed the models combining the damage model and distribution function, also few others [11,12,36,38] combined the life prediction model with it.

A limited work by Miner et.al. [3] on fatigue of Kevlar-49 fiber composites shows that the tension-tension fatigue resistance of unidirectional Kevlar fiber composite (Fig. 1.1) is comparable to that of unidirectional boron fiber composite,

which is recognized as best among composite materials. The advantage over GRP and a conventional aluminum is significant. They also found out the fatigue resistance of Kevlar-49 fabric reinforced epoxy composite as better than comparable glass fabric reinforced epoxy composite. They found the fatigue properties of Kevlar composites as much sensitive to strain rate. Other useful works on Kevlar have been done by investigators [5,39-43]. Clements [39] stated the difficulties in fabrication of Kevlar fiber composites and in cutting of laminates. Bunsell [5] have determined the tensile and fatigue behaviour of Kevlar-49 bare fiber. He found narrow hysteresis loop inf fatigue cycling after few initial cycles. Clements et.al. [40] have obtained the tension, compression and shear properties, of Kevlar composites. Although, they found, tensile and compressive elastic constants same, the material proved to be several times (approximately five times) stronger in longitudinal tension than in longitudinal compression, and also several times weaker in transverse tensile than in transverse compression. Jacob et.al. [41] found the static tensile strength and several types of failure modes for Kevlar/epoxy composite, testing ring type specimens. Zweben [42] and Fischer et.al. [43] shows that the bending behaviour of aramid fiber composites is affected by the large difference between the tensile and compressive strengths of the fiber. They have given an elastic-plastic model based on elastic-perfectly plastic compressive and elastic brittle tensile behaviours. The influence of the multi-modulus (different modules in tension and compression, mainly for carbon-carbon composite) characteristic

on the behaviour of a flexural test beam has been evaluated by Jones [44]. Any work on the flexural fatigue of Kevlar fiber composite material was not available. It was, therefore decided to perform the flexural fatigue tests on Kevlar fiber reinforced epoxy composites.

1.4 PRESENT WORK:

In the present investigation Kevlar-49 fabric reinforced epoxy resin composite laminates were fabricated by hand lay-up technique in the laboratory (described in Sec. 2.1). The specimens of the required size have been prepared by sectioning the laminate with circular saw (Sec. 2.2). The static flexural tests were performed for static characterization on MTS under three point bending (Sec. 2.3). The fatigue testing machine available in the Composite Materials Laboratory, designed, fabricated, and used earlier by Joneja [18] was modified and used for present investigation. The testing system is described in Sec. 2.4. The flexural fatigue tests in cantilever loading were performed on flat specimens. One end of the specimen was fixed while the other end was cycled between known displacement limits with zero mean displacement. The different displacement limits, namely 12, 13, 18, 21 and 26 mm etc. were selected so that the fatigue life varied from about a thousand to a half million cycles. The bending moment at the fixed end was measured by means of a dynamometer and was recorded at desired intervals without interrupting the fatigue tests. The whole experimental

procedure is described in Section 2.5. Fracturographic study of a specimen was performed under microscope and described in Sec. 3.1 alongwith the failure criterion of specimens in fatigue. Damage accumulation with number of cycles was studied and a damage model was developed (Sec. 3.2). Analytical model of S-N curve and its statistical analysis is described in Sec. 3.3. Conclusions drawn from the investigations and some suggestions for future work have been given in Sect. 3.4 and 3.5 respectively.

CHAPTER 2

EXPERIMENTATION

2.1 MATERIAL FABRICATION:

The present investigations have been performed on Kevlar-49 fabric reinforced epoxy resion. Although fabric material has low fatigue properties than unwoven material, it is widely used in practical applications due to ease of fabrication. Moreover, in the laboratory this was the only form of Kevlar-49 fiber available. Kevlar-49 fabric specifications supplied by the manufacturer are given in Table 2.1. Fabric has unequal counts and denier of fiber in cross-direction. It makes the fiber volume ratio in warp and fill direction as 10:1. This type of weaving is generally referred to as the unidirectional weave. All the properties calculated in the present study are for warp direction which is the dense fiber direction.

The specifications of the epoxy supplied by the manufacturer are given in Table 2.2. Curing temperature and corresponding curing times as suggested by manufacturer himself are given in Table 2.3. However, the different combination of curing temperature and time produces no observable difference in properties of composite.

Table 2.1: Kevlar Fabric Specifications.

Product	-	Du Pont Co., USA
Category	-	Kevlar-49 Fabrics
C.S. Style	-	343
Former Du Pont Style	-	143
Weight (per unit area of fabric), g/m^2	-	190
Tensile strength, N/m		
Warp	-	255700
Fill	-	28700
Count (No. of yarn/in. in warp x fill)	-	100 x 20
Yarn denier (Weight in g. of 30,000 ft. long yarn)		
Warp	-	380
Fill	-	195
Weave	-	Crowfoot
Finish	-	CS - 805
Fiber Properties:		
Specific gravity	=	1.44
Decomposition temp.	=	$500^{o}C$

Table 2.2: Epoxy Specifications.

Product		- CIBA Geigy India Ltd.
Category:	Resin	- Araldite LY556
	Hardner	- Hardner HY951 (10% of Araldite by wt.)
Mixing		- At room temperature
Viscosity, cp		- 5000 - 8000
Pot life, hr.		- 0.5 - 1.00
Specific gravity		- 1.2 - 1.3
Tensile strength, MPa		- 55 - 130
Tensile modulus, MPa		- 2800 - 4200
Poisson's ratio		- 0.20 - 0.33
Flexural strength MPa		- 125
Decomposition temp. °C		- 270 - 280

Table 2.3: Epoxy Curing Chart.

Curing Temp. (°C)	Curing Time
20	14 - 24 hr.
50	5 - 7 hr.
80	1 - 2 hr.
100	15 - 30 min.
140	5 - 10 min.

Composite laminates of 3 mm thickness were cast by hand lay-up technique in the laboratory. Fabric was cut into the required size by a special Kevlar cutting scissors, supplied by fabric manufacturer Du Pont Company itself. The fabric size was kept such that a good central portion of 250 x 170 mm^2 size could be obtained. To obtain maximum fiber volume fraction along with good surface finish, ten layers of fabric were used for 3 mm thick laminate. Fabric was demoisturized completely by pretreating it in an oven at 105°C for 16 hours. It was then cooled in the oven itself so that no moisture could be absorbed again.

Composite laminates were cast between two 25 mm thick mild steel mould plates lined with mylar sheets. These mould plates were got chromium plated to avoid rusting and hence to ensure the good surface finish of the laminates. The mylar sheets make it easy to release the laminate from plates and also ensures the good surface finish. The fabric pieces were placed on the lower mould plate one by one. Resin was spread on lower mould plate and on the top of each fabric piece and spread by means of a brush. To enhance wetting and impregnation the resin was tapped and dabbed with spatula before spreading resin over fabric pieces. The laminate was rolled gently with a rubber roller after placing mylar sheet on the top. This squeezes out the entrapped air and the extra epoxy. The upper mould plate was then placed on the top. The mould plates were separated by mild steel spacers to control the

thickness of the laminate. The mould plate applies a pressure due to its own weight and due to tightening of nuts on the bolts going through both the mould plates. Excess resin gets squeezed out from the sides.

The plates were cured at room temperature for about 6 hours and then at 55 - 60°C for another 12 hours by heating the mould plates through several 250 W heating elements placed on the outer surface of each mould plates. The rate of heating could be controlled through a transformer.

There is no easy method of finding the fiber volume fraction, experimentally for Kevlar fiber composites, because in the resin burn-off test, the fibers also burn off [39]. Other methods are tricky, therefore, following indirect method is used to calculate the fiber volume fraction;

Weight of fabric impregnated in a known volume of composite can be easily calculated by the areal density of the fabric. Thus fiber volume fraction can be calculated if fiber density is known.

Fiber volume fraction -

$$V_f = \frac{AN\rho_{fa}/\rho_f}{At} = \frac{N\rho_{fa}}{t\rho_f}$$

where,

A : Area of composite laminate.

N : Number of fabric layer in laminate

= 10

ρ_{fa} : Areal density of fabric
= 0.190 kg/m^2

ρ_f : Density of fiber
= 1.44 x 10^3 kg/m^3

t : Thickness of laminate
= 0.003 m

Hence,

$$V_f = \frac{10 \times 0.190}{0.003 \times 1.44 \times 103}$$

$$= 0.4393 \quad (\simeq 44\ \%)$$

2.2 SPECIMEN PREPARATION:

Cutting of Kevlar composite is a difficult job. Clements [39] suggested the sectioning of laminates by a fine-grit diamond wheel at low speed. However, by this method the speed of cutting is too slow. Cutting by router at speed of 10,000 and 45,000 rpm produced a lot of brooming at the edge. Cutting with a low power laser beam burn off the edges. These brooming and burning at edges can not be accepted for fatigue tests. Water jet cutters are probably the best but are not available in the laboratory.

In mechanical cutting of Kevlar composites, a lot of problems are a direct consequence of the fiber toughness. Because of its high toughness and strength, the fibers break and pull out from inside of the composites instead of cutting at the edge. This problem is more at low cutting speeds.

The best results in cutting laminates was obtained in circular sawing when unconventional side (slant side of teeth) of a metal slitting fine teethed H.S.S. cutter was used at high speeds [45]. Cutter size used is 6 in. dia. and 2 mm thickness with 7 - 8 teeth per inch which would be better if finer. Circumferential speed of cutter is around 30 m/s with plenty of cooling water. The cutting speed in dense fiber direction (cutting less fibers) is quite high but in cross-direction it is moderate. The quality of the edge is quite good except few broomed fibers at one side of edge from which cutter comes out after cutting. This brooming can be easily removed by sanding the edges on simple wood sanding paper and a good edge finish obtained.

2.3 PRILIMINARY MATERIAL CHARACTERIZATION:

Static flexural properties of the material were obtained by three point bending tests on MTS. Two specimen of 150 mm length, 12.7 mm. width and 3 mm thickness were tested with 100 mm span. Load was applied at centre span and load versus deflection curves plotted. The typical curve is shown in Fig. 2.1. The average properties calculated by simple beam theory are given in Table 2.4.

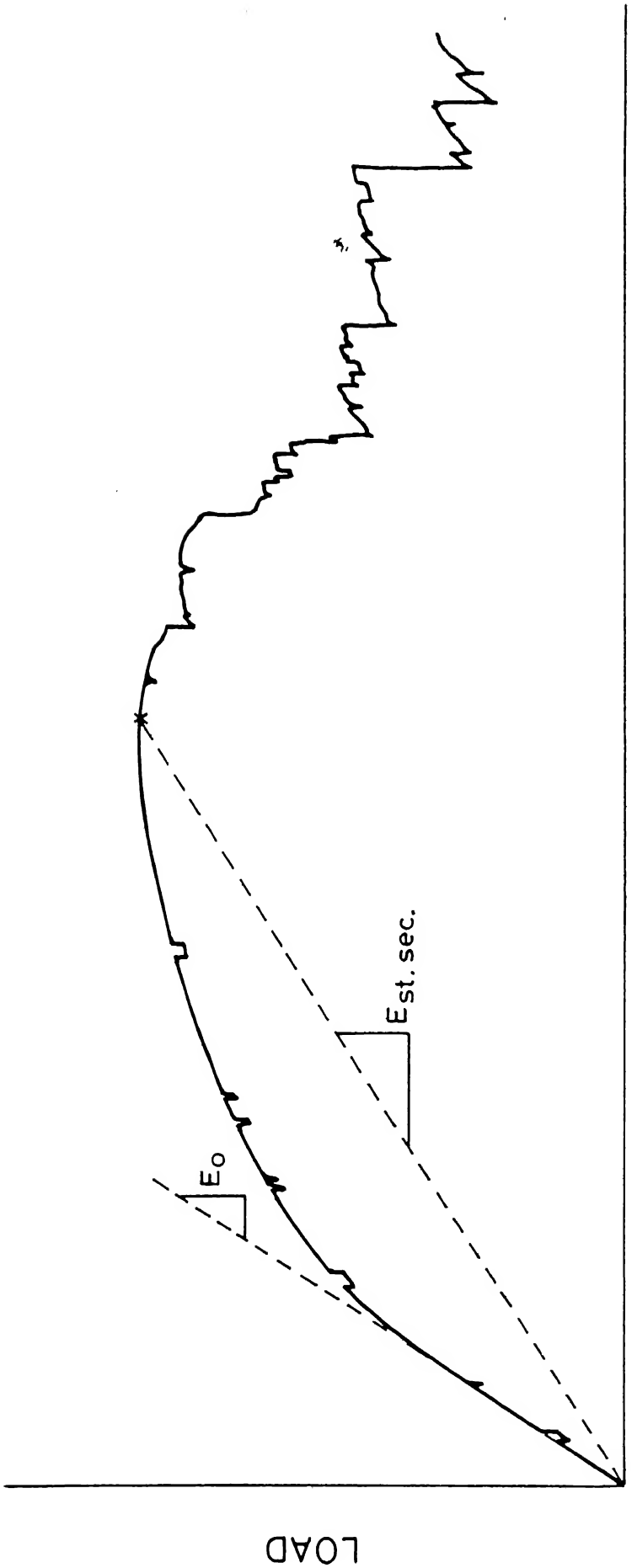

Fig. 2.1 Static flexural stress - strain curve (three point bending, stroke control mode)

Table 2.4: Static Flexural Properties of Material.

Proportional Strain	$\mu m/m$	5850
Proportional Stress	MPa	257.50
Tangent Modulus E_o	GPa	44.01
Ultimate Strain ε_u	$\mu m/m$	27450
Ultimate Strength σ_u	MPa	502.07
Secant Modulus $E_{st.sec.}$	GPa	18.29

NOTE: all the properties are for dense fiber direction.

2.4 TESTING SYSTEM:

In many applications, composites are subjected to the repeated bending loads which necessitate the flexural fatigue testing of composites. For Kevlar composites tensile and compressive strengths are different so that their flexural fatigue testing is of great importance. It was, therefore, decided to conduct fatigue tests in flexural mode. The advantages of flexural fatigue testing are the simplicity of specimens (hence inexpensive) and the fact that it is usually possible to conduct the tests at higher speeds because the specimen area which gets heated during cyclic loading is close to the surface. The disadvantages include the variation of stresses through thickness and along thelength as well. In flexural fatigue tests inter-laminar shear stresses are present which may cause delamination prior to tensile or compressive failure. However, these interlaminar stresses can be made

insignificant by proper selection of the span to depth ratio.

The fatigue testing machine available in the Composite Materials Laboratory andused in the present investigations had been designed, fabricated, instrumented and used earlier by Joneja [18]. However, some modifications were made in the system. The machine is designed for cyclic flexural loading. In this set-up, the specimens are fixed at one end while the other end is cycled between known transverse displacement limits (displacements perpendicular to the plane of the specimen) with zero mean displacement. This cycling produces alternating tensile and compressive bending stresses in the specimen.

The testing machine is schematically shown in Fig. 2.2. One end of the specimen is fixed in grips (b) which in turn are mounted on a dynamometer (a). The grips were designed to ensure proper gripping and alignment of the specimen. The dynamometer, on which the grips are mounted, had been designed to measure the bending moment at the fixed end of specimen. The dynamometer is an extended octagonal ring type and will be described later. The dynamometer is mounted on a rigid column whose base is fixed in the foundation.

The second end of the specimen is placed in a specimen holder (d) through which transverse displacement is provided to it. The design of specimen holder has been modified and will be described later. The specimen holder is mounted on a

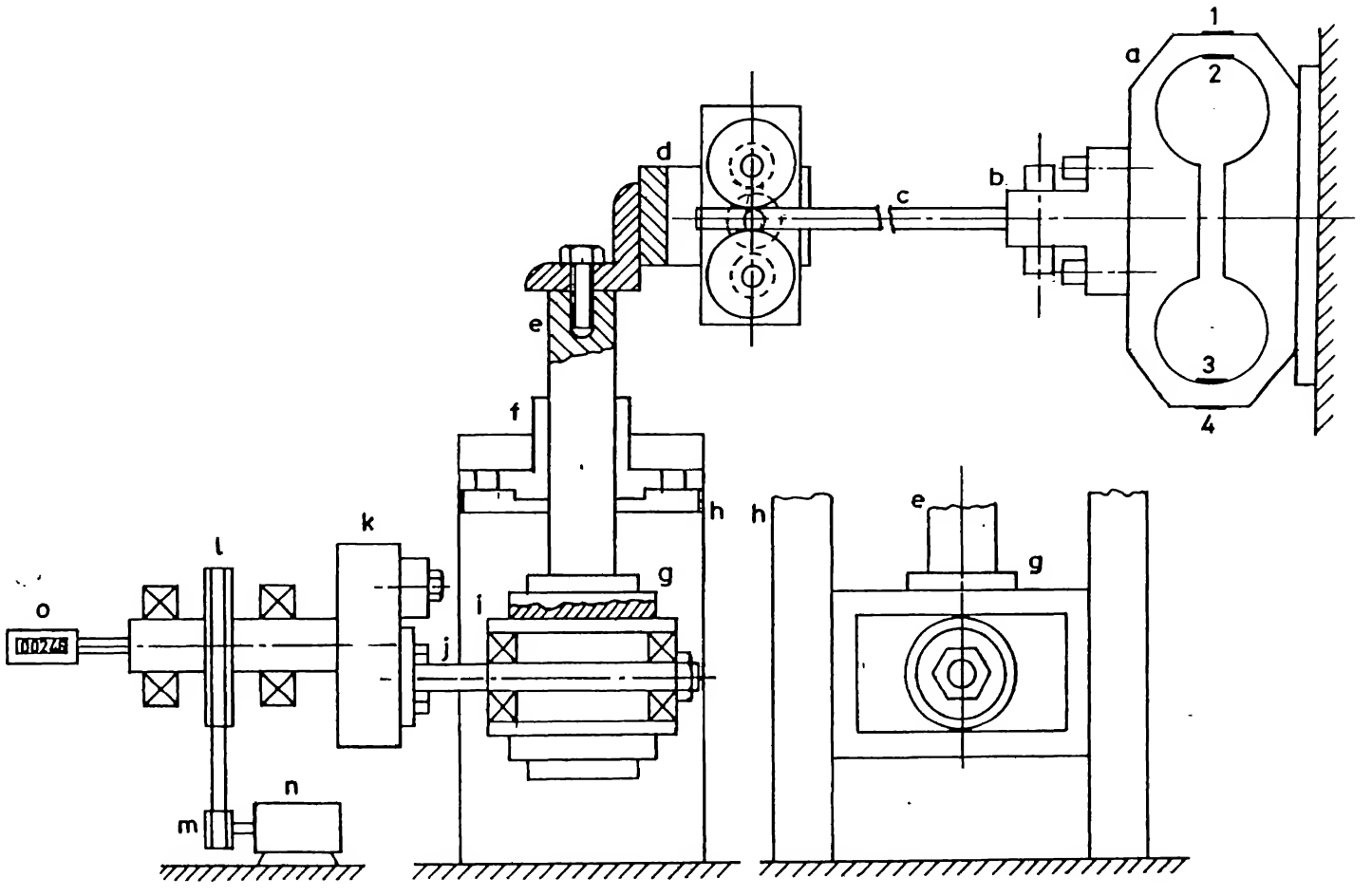

1, 2, 3, 4 - Strain gauges; a - Dynamometer; b - Specimen grips; c - Specimen; d - Specmen holder; e - Cylindrical rod; f - Teflon bush; g - Rectangular guide; h - Rectangula guide constraints; i - Eccentric pin roller; j - Eccentric pin; k - Driving disc; l - Driving pully; m - Motor pully; n - Motor; o - Counter.

Fig. 2.2 Schematic diagram of flexural fatigue testing machine.

cylindrical rod (e) which is reciprocated by a driving link mechanism. Details of the driving link are illustrated through two different views in Fig. 2.2 itself. At the lower end of the cylindrical rod, a rectangular box (g) is attached, which moves with it. Movement to the box is provided by a roller (i) which moves in the box freely. The roller is attached to a pin (j) eccentrically mounted on the driving disc (k). With this arrangement vertical reciprocating motion of the pin is transferred to the specimen holder through the box and the cylindrical rod but its horizontal motion is not transferred due to horizontal rolling of the roller in the box. The rectangular box moves vertically between two guides (h). Movements of the rod other than the vertical are constrained by moving it in a teflon bush (f).

The amplitude of displacement of the rod (hence of the specimen) from neutral position is equal to the eccentricity of the pin. Thus, amplitude of displacement can be changed by changing the eccentricity. It may be noted that the vertical motion of the specimen end thus obtained is simple harmonic so that the changes in velocity and acceleration are smooth. Simple harmonic motion also provides a low strain rate near maximum strain and high strain rate near neutral position.

Drive to the disc is provided by an electrical motor through a belt and pulley arrangement. The disc is so thick that it also acts as a flywheel to smoothen the motion. The

speed of disc (hence the loading frequency) can be changed by changing the size of the pulley on the motor shaft. Digital counter is employed to register the number of cycles.

The two most important parts of the machine are described here. These are the dynamometer and the specimen holder through which its free end is moved. The specimen holder has been designed such that the ideal loading conditions as shown in Fig. 2.3(a) can be achieved. The ideal loading condition requires that the point of action of load at neutral axis of the specimen should remain at a constant distance from fixed end, even in the deformed position. Loading at free end deforms the straight specimen to a curved shape, so that the free end moves towards the fixed end, as shown in Fig. 2.3(a). Thus to keep the distance of point of action of load constant, it should shift along the specimen length away from fixed end. In the present design, the specimen is loaded by means of two rollers, one roller each for applying load in either direction (Fig. 2.3(b)). To maintain a fixed distance of inter-section point of the load action line (i.e. the line joining the centre of the load applying roller and loading point) and the neutral axis from fixed end, the rollers are permitted to move over the specimen, to shift loading point. It may be emphasized here that these rollers should not squeeze the specimen in the thickness direction (this promotes transverse splitting of the specimen), introduce

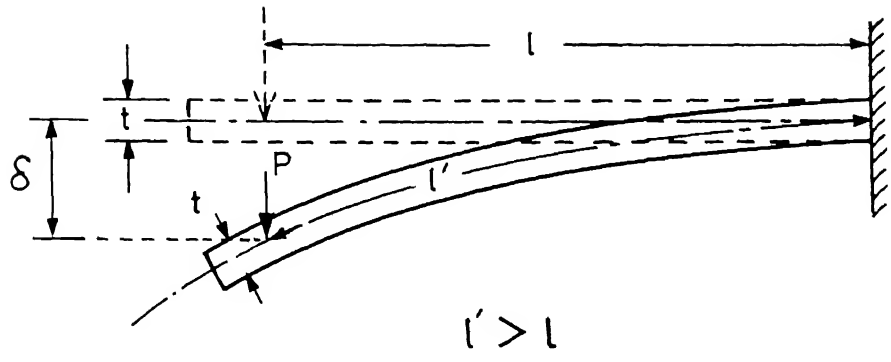

(a)

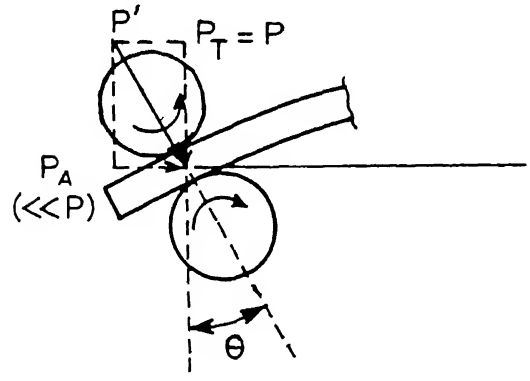

(b)

Fig. 2.3 Loading of specimen
(a) Ideal specimen loading
(b) Loading by two rollers.

no bending at the free end, and no axial force is produced. To satisfy the first two requirements when one roller applies load, the other roller should move such that no squeezing or bending occur at free end. This can be achieved by rotating both the rollers around loading point at neutral axis, so that the line joining the centres of the roller remained perpendicular to specimen. To avoid axial force in the specimen, the rollers should roll on the specimen rather than slipping on it. However, a smallaxial force (P_a) is unavoidable because of the specimen curvature as shown in Fig. 2.3(b).

The required functions of the holder has been achieved in modified design. Schematic diagram of modified holder is shown in Fig. 2.4(a) and its functioning is shown in Fig. 2.4(b). Both ends of the rollers are mounted in bearings, so that they can roll over the specimen. These bearing on both side of rollers are mounted in two plates keeping the space between rollers equal to the thickness of specimen. These plates are again mounted by means of centrally extended pins in two bearings which are mounted in a U type frame. This frame is bolted on reciprocating circular rod. The plates, on which rollers and bearing are mounted, can rotate along with the rollers so that deformation of specimen could be accommodated without producing any bending at specimen free end. The specimen holder with rotated rollers is shown in Fig. 2.4(b), which clearst the functioning of the holder. The photograph of the specimen holder is given in Fig. 2.5.

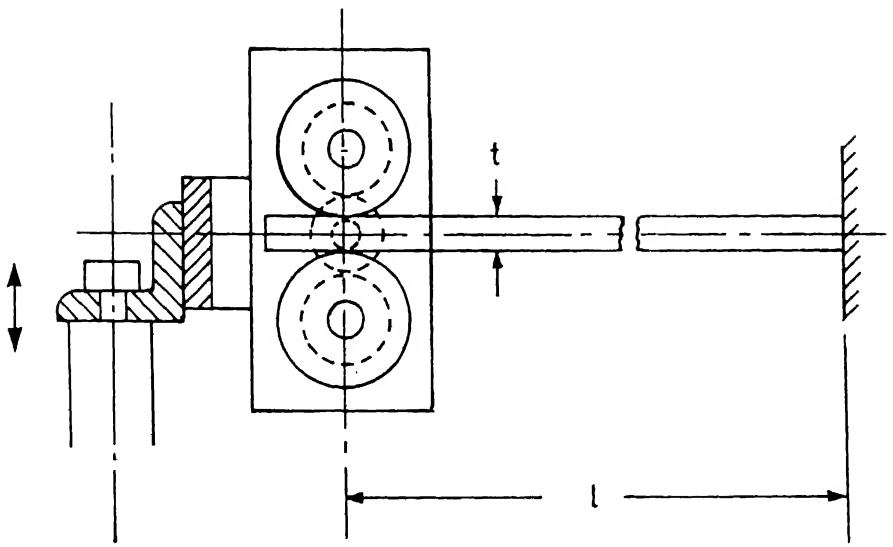

(a)

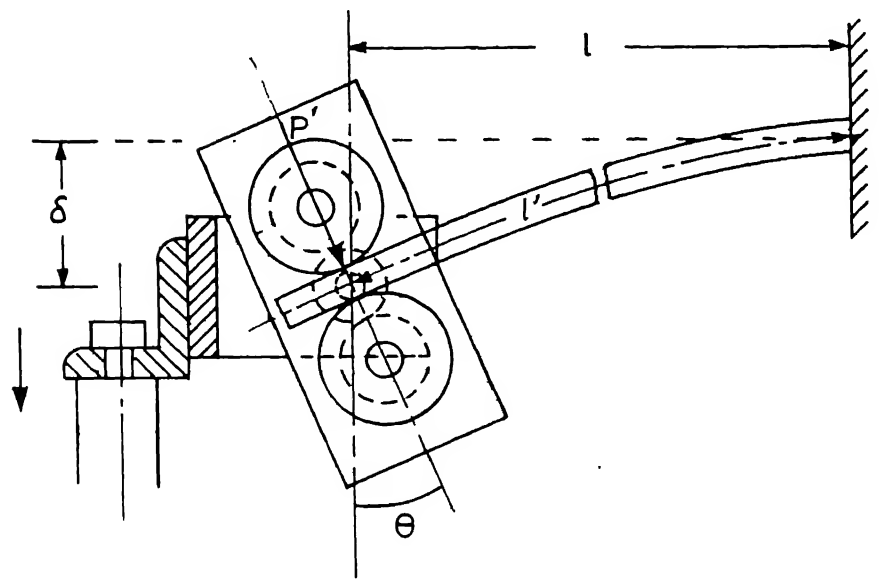

(b)

Fig. 2.4 Schematic diagram of specimen holder
(a) Neutral or mean position
(b) Tilted position.

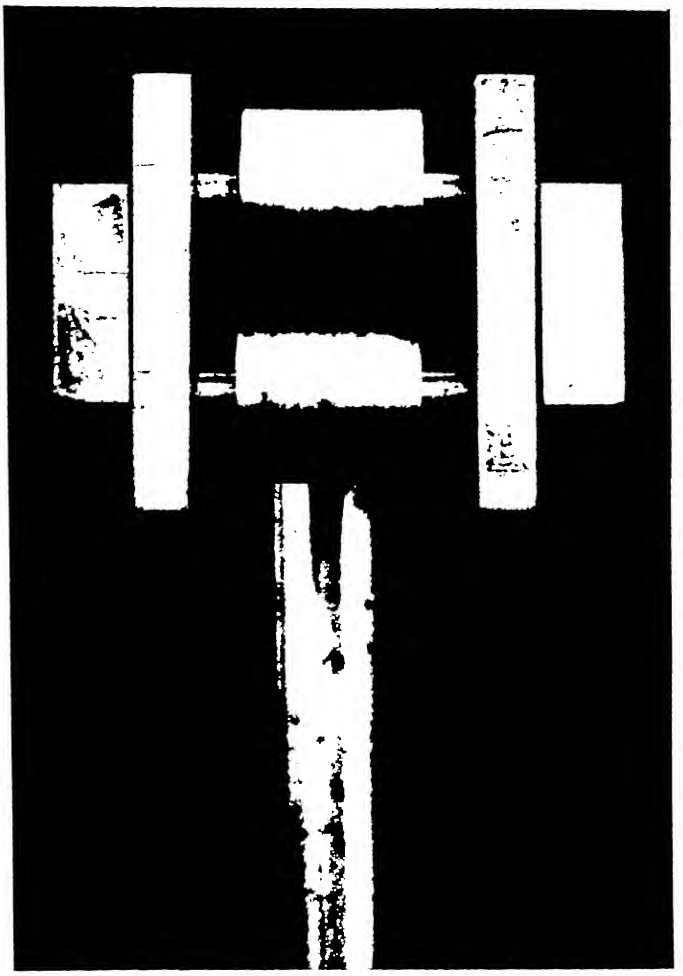

Fig. 2.5: Specimen holder.

The dynamometer had got rusted and the strain gauges had come out. Therefore the dynamometer has been cleaned and chromium plated. The chromium plating was thin enough to ensure proper functioning of strain gauges. Four foil type electrical resistance strain gauges (A product of BLH Electronics, USA, Type FAE-25-12-56 EWL, length = 6.35 mm, GF = 2.02 $\pm$ 1 %, K = -0.3 %, Resistance = 120 $\pm$ 0.2 ohms) with anchore tabs have been employed on dynamometer and protected by micro-acrylic wax coating from environmental attach. The strain gauge positions are shown in Fig. 2.2, itself. The strain gauges have been connected to form a Wheatstone bridge (as shown in Fig.2.6), such that the output of the bridge is proportional to bending moment at the fixed end.

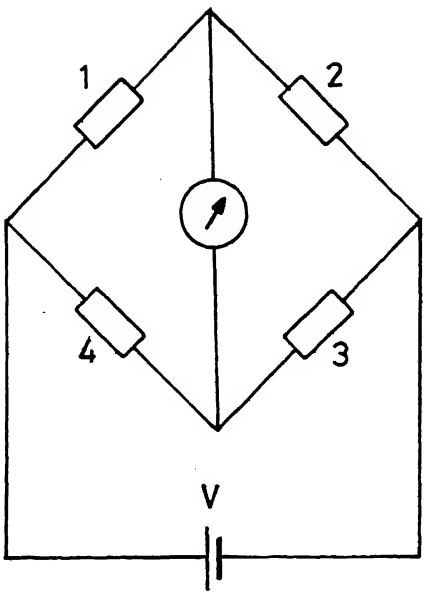

Fig. 2.6 Wheatstone bridge

The output of the bridge,

$$\Delta E = \frac{1}{4}\frac{V}{R}(\Delta R_1 - \Delta R_2 + \Delta R_3 - \Delta R_4)$$

where,

V : applied voltage,

R : resistance of gauge,

ΔR's : the change in the resistances of strain gauges.

The changes in the resistance of strain gauges 1 and 3 are added up and the changes in the gauges 2 and 4 are subtracted in the output of the bridge.

The load P' applied by rollers on specimen free end can be resolved into two forces, a transverse load P_T and an axial force P_A, as shown in Fig. 2.7(a). The transverse load P_T at the free end results in a transverse load P_T and a moment $P_T l$ at the fixed end. Similarly the axial load P_A at the free end results in an axial force P_A and a moment $P_A \delta$ at the fixed end as shown in Fig. 2.7(e). All the forces and moment at fixed end will produce separately a transverse force, a axial force and a moment at the horizontal arms of octagonal dynamometer as shown in Fig. 2.7(c), (d), (f) and (g).

The transverse forces will not produce any effect on strain gauges since an axial force will produce equal streams in strain gauge 1 and 2 and the strain in 3 will be equal to 4.

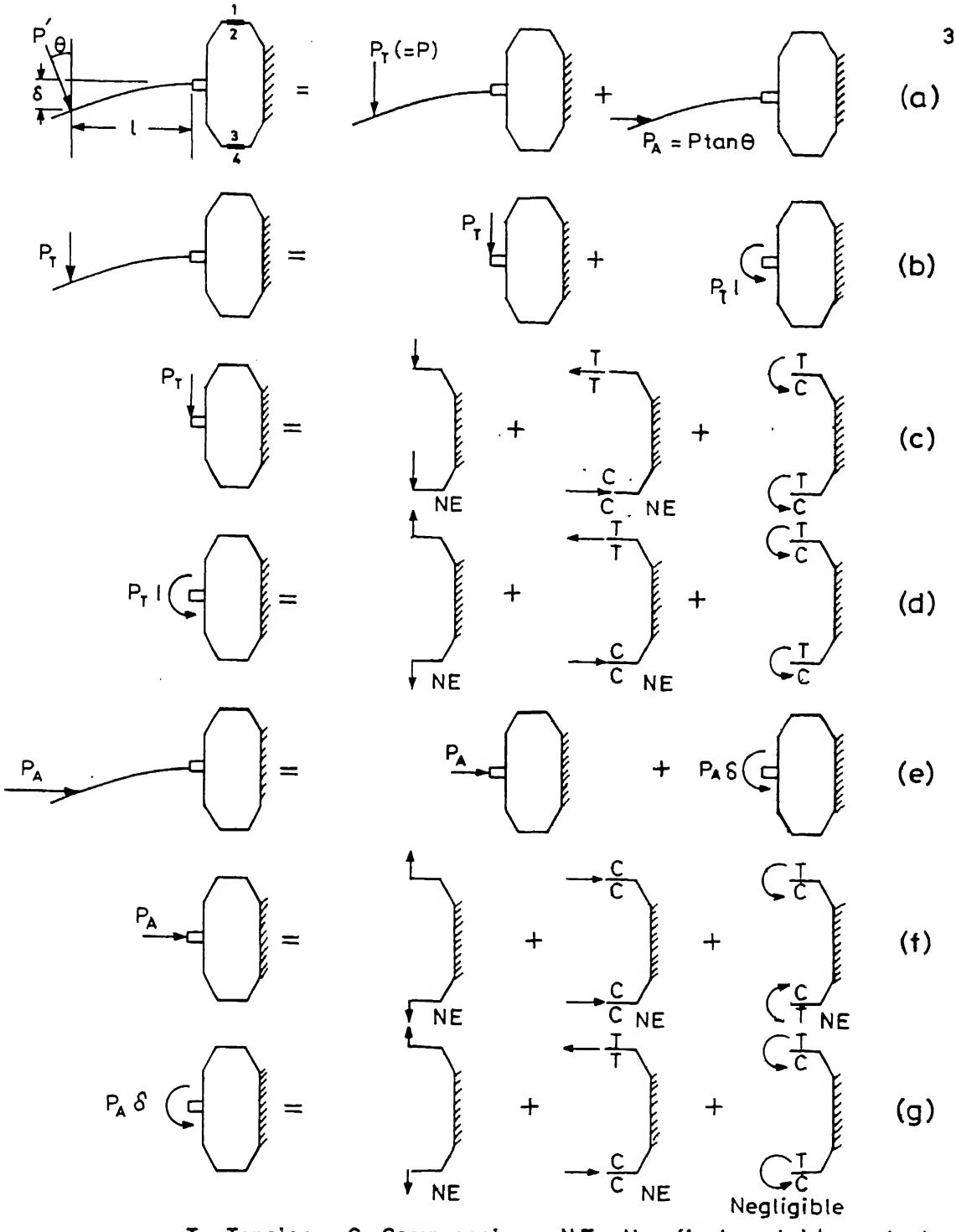

T - Tension, C - Compression, NE - No effect on bridge output

Fig. 2.7 Dynamometer loading analysis.

They will thus cancel each other in the output of bridge, thus there will be no effect of any axial force at horizontal arm of dynamometer on the bridge output. The bending moment produced in horizontal arms by the force P_T and the moments $P_T l$ and $P_A \delta$ are in the same direction but bending moment in horizontal arms because of P_A is in the opposite direction and equal to each other. Equal bending moment in opposite direction will produce equal strain in strain gauge 1 as in 4 and also equal strain in 2 as in 3, as shown in Fig. 2.7(f). They will, thus, again cancel each other in bridge output hence no effect of axial force P_A. Bending moments in same direction will produce the equal strains of opposite natures in strain gauges 1 and 2 and similarly equal strains of opposite natures in 3 and 4. Also the strains in 1 and 3 are of same nature and also strains in 2 and 4 are of same nature which result in addition of all strains as output of bridge. Thus the forces P_T and moments $P_T l$ and $P_A \delta$ effect the bridge output. As δ is too small as compared to l, the tilt θ is also small which results in a much smaller force P_A as compared to P_T. Hence effect of moment $P_A \delta$ on bridge output cank be neglected. Thus if l is a constant, the bridge output will become proportional to transverse load P_T and hence proportional to moment at fixed end $P_T l$.

Since arms of the bridge have active identical gauges, the bridge is automatically temperature compensated. Thus the

output of the bridge is proportional to only the transverse load applied at free end of specimen, and hence the bending moment at fixed end for fixed specimen length.

In the beginning the bridge output was measured by a Tetronix 531 oscilloscope with plug in unit type Q. But an oscillograph visicorder was preferred due to high sensitivity and ability to record. The dynamometer has been calibrated using a mild steel specimen. Increasing loads through standard weights were applied at a known distance l from fixed end. Bending moment at fixed end was calculated from the geometry. Plots of the bridge output in strain unit are shown as a function of transverse load at fixed distance from fixed end and bending moment at fixed end in Fig. 2.8. It can be seen that the calibration curve is linear upto the applied load which are much more than the load expected during fatigue tests.

Overall view of modified system is shown in photograph of Fig. 2.9.

2.5 EXPERIMENTAL PROCEDURE:

Modes of loading and Control:

Flexural fatigue tests have been performed on flat specimens prepared from the material fabricated in the laboratory. The mode of loading was cantilever beam type. One end of the specimen was fixed in the grips mounted on a dynamometer while other

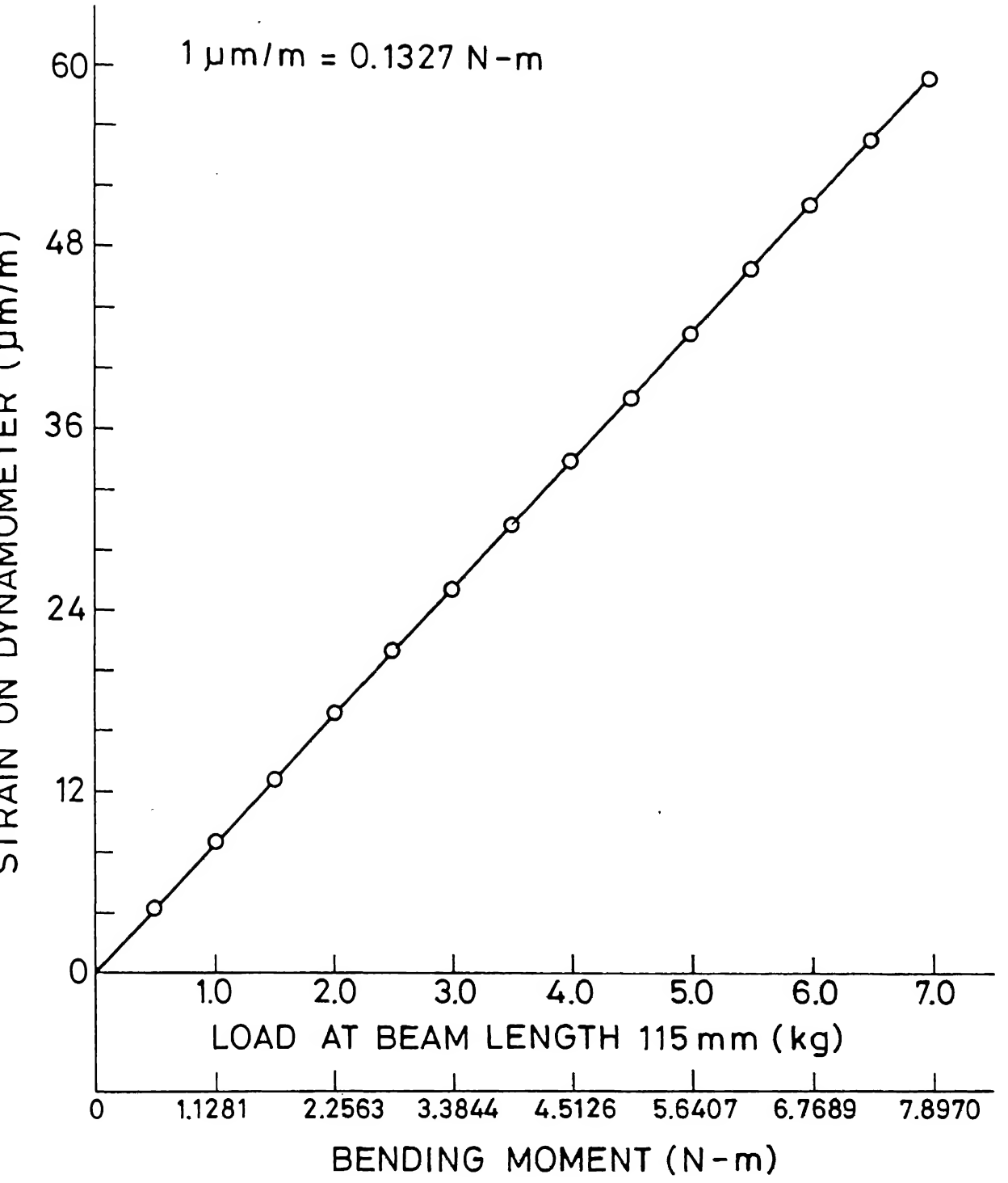

Fig. 2.8 Calibration curve of dynamometer

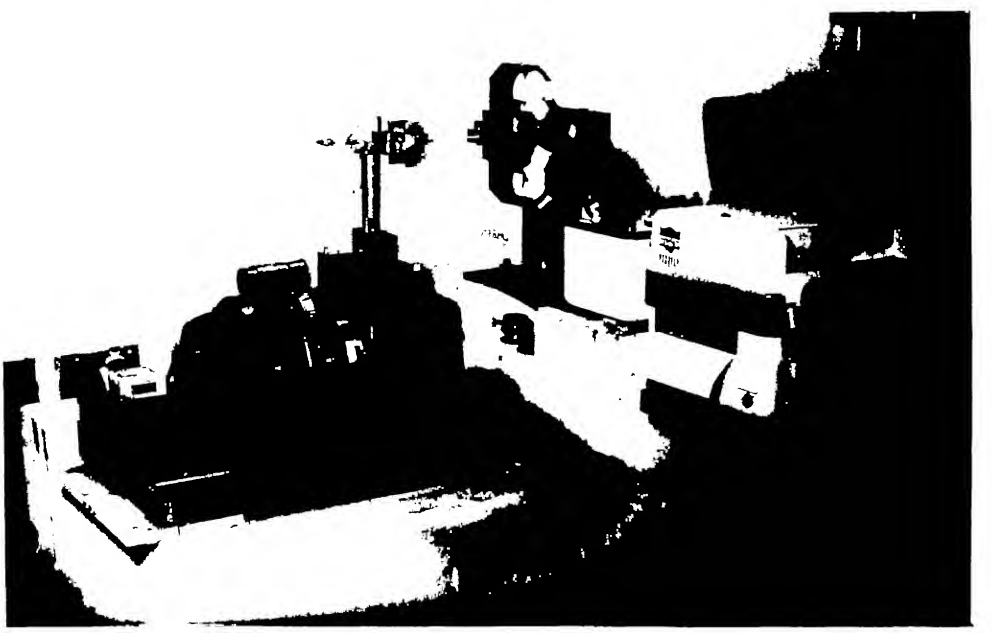

Fig. 2.9: An overall view of the testing system.

end was cycled between known displacement limits with zero mean displacement. As displacement controlled mode is less damaging as compared to load controlled mode, the fatigue life for specimens tested in displacement controlled is higher. Thus better and easier study of damage is possible with stroke control mode. However, the damage mode or fatigue failure mechanism is not affected by the control modes [21]. The different displacement limits (26, 21, 18, and 13 mm. etc.) were selected so that fatigue life varied from about a thousand to six lacks cycles. A number of specimens (approximately 9) were tested at each displacements to obtain full scatter band of fatigue life.

Specimen Dimension:

To obtain the correct value of flexural strength the dimensions of the specimen should be such that the failure takes place by breaking of fibers and not by interlaminar shear. Keeping length to thickness ratio high, the interlaminar stresses can be minimized. But large length to thickness ratio requires large deflection at the free end which in turn develops unwanted horizontal forces. Thus keeping both the things in mind the length to thickness ratio has been kept approximately forty. Specimen dimensions are shown in Fig. 2.10.

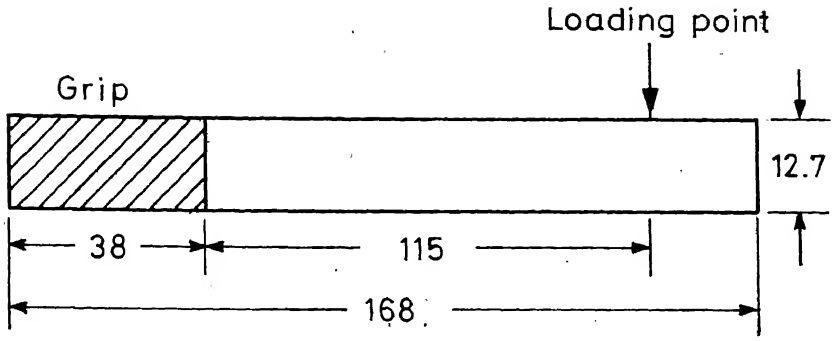

All dimensions in mm

Fig. 2.10

Frequency:

Cyclic loading causes a heating of the specimens due to internal friction. Increase in specimen temperature is larger for higher strain rate. However, it is negligible when strain rate is below a particular level [21]. Whereas for same stain rate, temperature increase is higher at higher strain amplitude [11]. Thus, the rate of cycling has a strong effect on the low cycle fatigue life whereas the effect is less pronounced at higher number of cycles [15], although, fatigue failure mechanism is not affected by the cyclic frequency [21]. Therefore, low frequencies have been used at high cyclic strains and high frequencies at low cyclic strains. At higher frequencies it was seen that the damage occurs away from the fixed end instead of at fixed end. Thus frequencies have been chosen such that the damage occurred at fixed end. However, due to experimental limitation, the frequency at highest displacement (i.e. 26 mm)

was kept as 5 cps, even though the damage occurred slightly away from fixed end.

Damage Measurement:

The character and extent of internal damage has been studied by investigators using different methods. Optical and electron microscopy are the direct methods. Nondistructive inspection techniques are now being developed fordetection of fatigue damage. These techniques include ultrasonic, holography interferometry, X-ray radiography and acoustic emission etc. Change in structural properties such as static or dynamic modulus, residual strength, stress, strain and temperature during fatigue loading are also considered indicative of internal damage. Internal cracking results in the lowering of the stiffness and strength of composites. Tanimoto and Amijina [9,30], Agarwal and Joneja [19,20] and Joneja [18] have related the changes in residual strength and modulus to the development of cracks in composites. Dally and Agarwal [7] developed a quantitative relationship between fatigue secant modulus change and crack density for composites. Many other investigators [10,11,14,18-21,26 were used fatigue secant modulus degradation as a measure of damage. Cessna et.al. [16] and Kim and Ebert [21] were performed constant deflection flexural tests monitoring the load decay (proportional to modulus decay) with cycles.

To measure residual strength or modulus the experiments have to be stopped or discontinued in between whereas fatigue

secant modulus can be monitored without interrupting the experiments. Thus bending moment (proportional to modulus) at the fixed end was measured by means of the dynamometer and was recorded in a visicorder at desired intervals without interrupting the fatigue tests. The point, at which the fatigue secant modulus reaches the static secant modulus, has been considered asfracture point. The experiments was discontinued at that point. Microscopic examination of a specimen was done in few steps upto final fracture.

CHAPTER 3

RESULTS, ANALYSIS AND DISCUSSION

Investigations have been carried out on Kevlar fabric reinforced epoxy resin laminates fabricated in the laboratory. The flexural fatigue tests were performed on flat specimens. One end of the specimen was fixed while the other end was cycled between known displacement limits with zero mean displacement. The different displacement limits, namely 12, 13,18, 21 and 26 mm. etc. were selected so that the fatigue life varied from about a thousand to a half million cycles.

Since the displacement to the free end of specimen was given by a eccentric pin rotating with constant speed, the strain cycle was sinusoidal as shown in Fig. 3.1. The fatigue stress cycle is similar to the strain cycle. The maximum stress and strain have been referred to as fatigue stress and strain respectively. These are also equal to the stress and strain amplitudes, because, in the present fatigue cycling maximum deflection on either side of zero mean deflection is the same. The minimum strain,therefore will beequal to strain amplitude but with an opposite sign. The strain and stress amplitudes calculated by simple beam theory and the fatigue life, N_f, obtained are given in Table 3.1, for each specimen. The bending moment at the fixed end was measured by means of a dynamometer and was

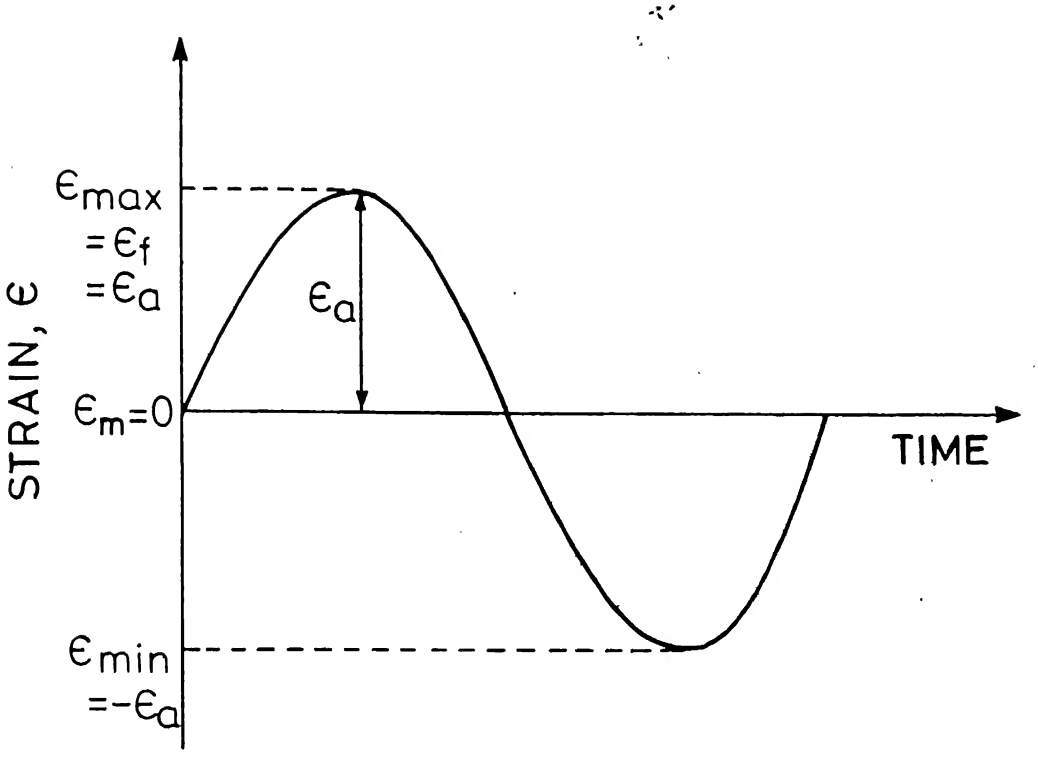

ϵ_{max} : Maximum strain
ϵ_{min} : Minimum strain
ϵ_f : Fatigue strain
ϵ_a : Strain amplitude
ϵ_m : Mean strain

Fig. 3.1 Fatigue strain cycle.

Table 3.1: Fatigue Data.

Specimen No.	Thickness t (mm)	Deflection δ (mm)	Fatigue strain, ε_f (μm/m)	Fatigue stress, σ_f (MPa)	First cycle fatigue modulus, $E_f(1)$ (GPa)	Fatigue life, N_f (cycles)
D12S1	3.25	12.00	4400	152.1	34.4	369000
D12S2	3.18	12.00	4328	153.4	35.4	680000
D12S3	3.22	12.00	4382	154.2	35.2	244300
D12S4	3.11	12.00	4233	147.5	34.8	690000
D13S1	3.18	13.00	4688	163.5	34.9	157500
D13S2	3.12	13.00	4600	160.2	34.8	249200
D13S3	3.16	13.00	4653	166.3	35.3	142500
D14S1	3.14	14.00	4986	171.7	34.4	126300
D15S1	3.22	15.00	5478	178.4	32.6	81600
D18S1	3.10	18.00	6328	212.0	33.5	39400
D18S2	3.15	18.00	6431	205.3	31.9	51500
D18S3	3.12	18.00	6369	202.9	31.8	41500
D18S4	3.11	18.00	6349	215.5	33.9	61300
D18S5	3.11	18.00	6349	212.3	33.4	48000
D18S6	3.12	18.00	6369	206.1	32.3	41450
D18S7	3.11	18.00	6349	207.4	32.6	49700
D18S8	3.06	18.00	6347	212.6	34.0	45300
D18S9	3.11	18.00	6349	211.5	33.3	52000
D21S1	3.02	21.00	7193	223.4	31.0	22200
D21S2	3.02	21.00	7193	244.0	33.9	12550
D21S3	3.02	21.00	7193	237.1	33.0	13000
D21S4	3.02	21.00	7193	233.7	32.5	15600
D21S5	3.14	21.00	7479	216.2	28.9	22300
D21S6	3.03	21.00	7217	235.6	32.6	11650
D21S7	3.11	21.00	7407	223.6	30.2	16650
D21S8	2.11	21.00	7407	226.9	30.6	14850
D21S9	3.02	21.00	7193	247.5	34.4	11750
D24S1	3.26	24.00	8874	249.7	28.1	6490
D26S1	3.26	26.00	9613	273.3	28.4	3930
D26S2	3.28	26.00	9672	259.3	26.8	3600
D26S3	3.28	26.00	9672	263.2	27.2	3590
D26S4	3.27	26.00	9643	264.8	27.5	3510
D26S5	3.26	26.00	9614	266.4	27.7	4110
D26S6	3.26	26.00	9614	271.3	28.2	3520
D26S7	3.26	26.00	9614	275.3	28.6	2710
D26S8	3.26	26.00	9614	266.4	27.7	3480
D26S9	3.25	26.00	9584	274.0	28.6	3660

$$\varepsilon = \frac{3t\delta}{2l^2}, \qquad = \frac{6M}{wt^2}, \qquad E_f = \frac{4l^2M}{wt^3\delta}, \qquad l = \text{Loading span length},$$

w = Specimen width, M = Bending moment at fixed end.

recorded at desired intervals without interrupting the fatigue tests. The fatigue secant modulus is the modulus at the maximum strain point (i.e. the ratio of maximum stress to maximum strain). It is calculated from the bending moment at the fixed end of the specimen by simple beam theory. The secant modulus for the first cycle is given in Table 3.1.

The reduction in fatigue secant modulus is taken in as a measure of damage in the present investigations. It was proposed to develop a damage model which represents the damage accumulation in the specimen with the number of cycles. Most of the damage models proposed in the literature required the damage and the number of cycles to be normalized to make the model simple. Thus the fatigue secant modulus, monitored during the tests, has been normalized with respect to difference in the fatigue secant modulus for the first and the last (N_f) cycle. The number of cycles have been normalized by the fatigue life. Normalizations have been done so that both the normalized quantities varied from zero to one. The normalized fatigue secant modulus is termed as normalized damage in the present work.

Normalized damage,

$$D = \frac{E_f(1) - E_f(N)}{E_f(1) - E_f(N_f)} \qquad (3.1)$$

where,

$E_f(N)$: the fatigue secant modulus at N number of cycles, and

N_f : Number of cycles to failure, i.e., fatigue life.

Normalized number of cycle,

$$N_{nor} = \frac{N - 1}{N_f - 1} \tag{3.2}$$

The normalized damage has been plotted against the normalized number of cycles for specimens at each displacements. Four specimens at 12 mm displacement and three at 13 mm were plotted jointly in Fig. 3.2. Nine specimens, each at 18, 21 and 26 mm displacements, were plotted in Fig. 3.3 to 3.5 respectively.

The fatigue life has been plotted on Log scale against the normalized fatigue strength and the normalized fatigue strain in Figs. 3.6 and 3.7 respectively.

Normalized fatigue strength,

$$\sigma_{nor} = \frac{\sigma_f}{\sigma_u} \tag{3.3}$$

where,

σ_f : fatigue strength

σ_u : static flexural ultimate strength.

Similarly, normalized fatigue strain,

$$\varepsilon_{nor} = \frac{\varepsilon_f}{\varepsilon_u} \tag{3.4}$$

where,

ε_f : fatigue strain, and

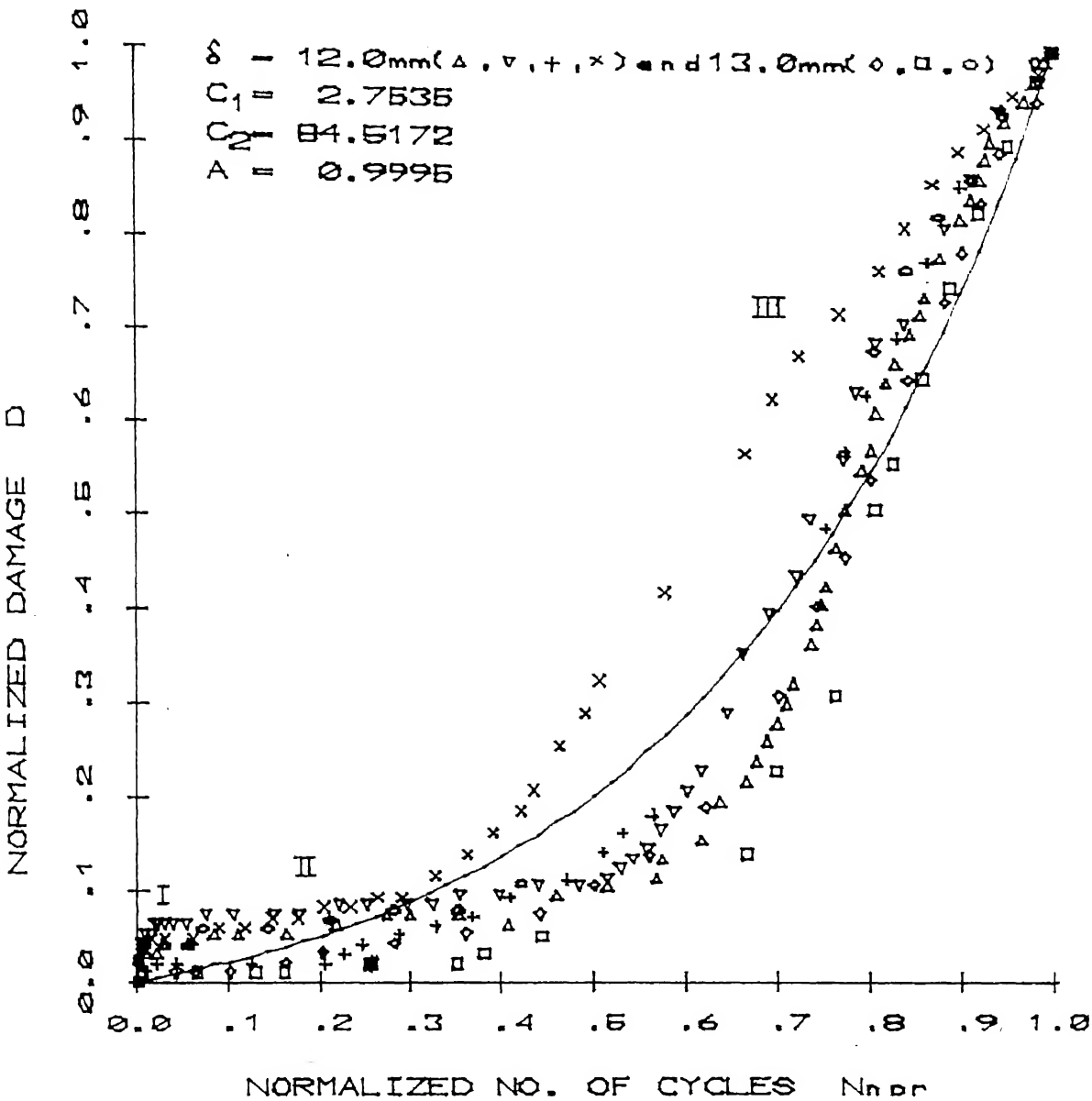

FIG.3.2 DAMAGE ACCUMULATION PLOTS (EACH SYMBOL REPRESENTS A SPECIMEN)

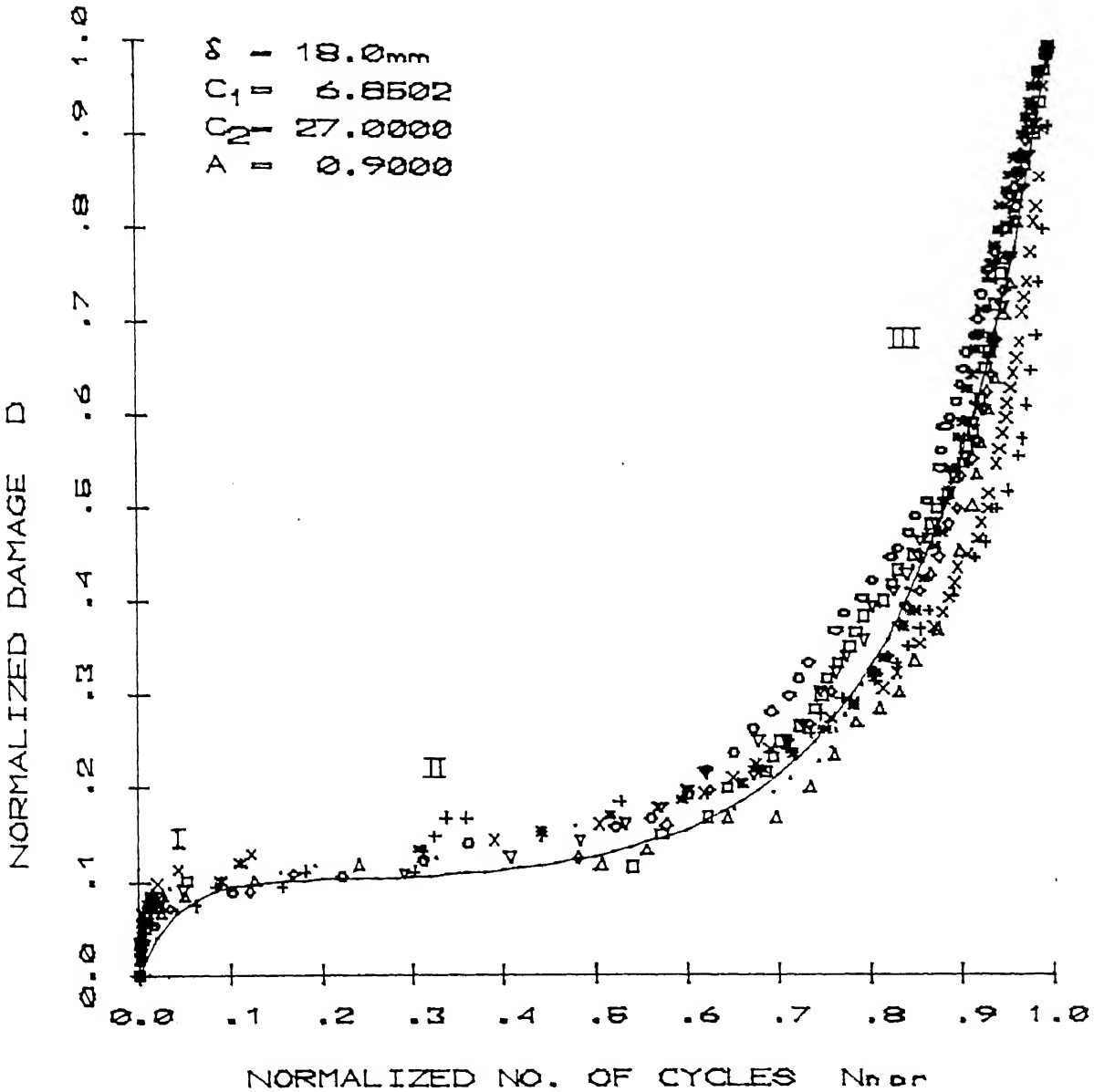

FIG.3.3 DAMAGE ACCUMULATION PLOTS (EACH SYMBOL REPRESENTS A SPECIMEN)

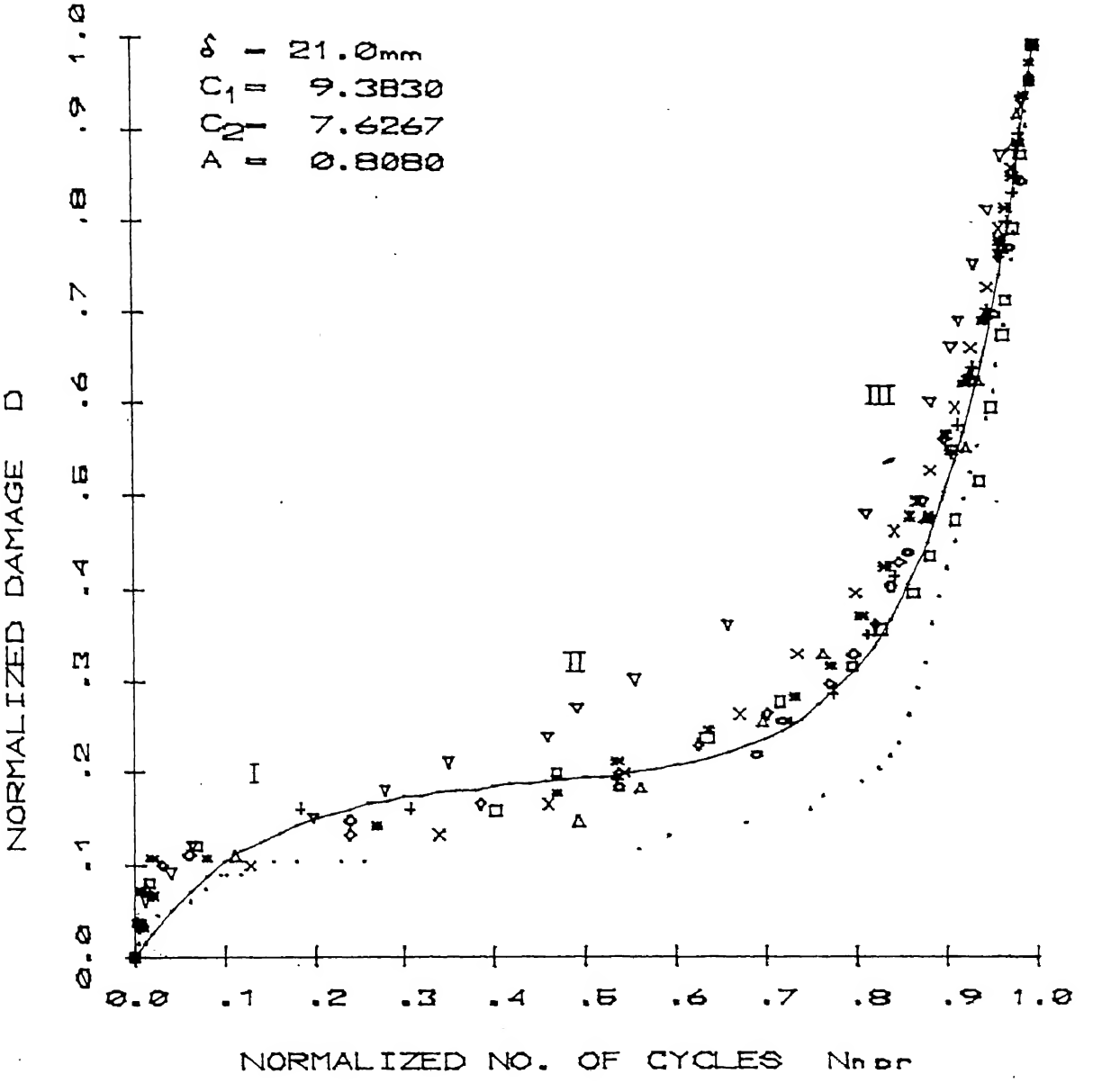

FIG.3.4 DAMAGE ACCUMULATION PLOTS (EACH SYMBOL REPRESENTS A SPECIMEN)

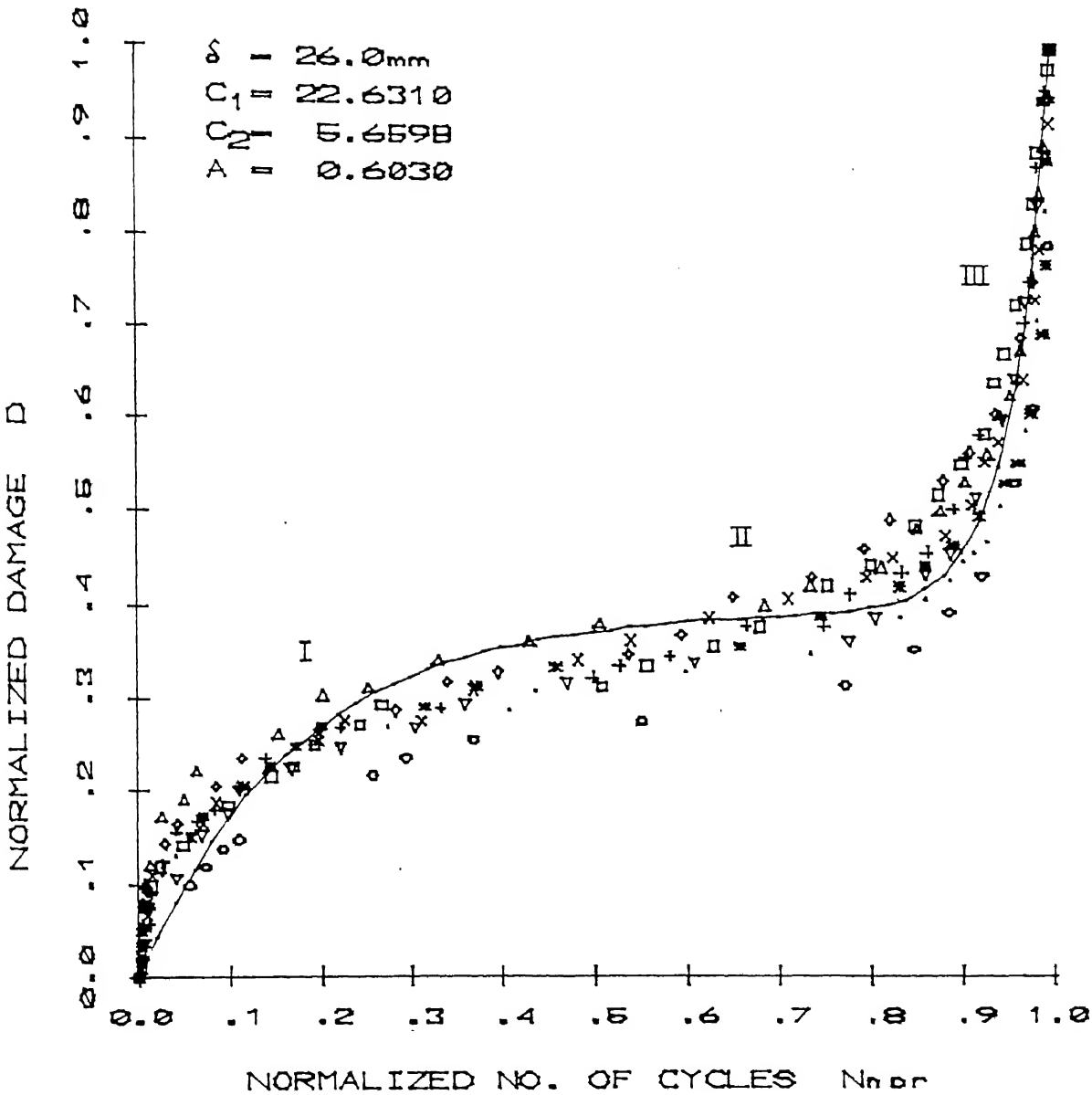

FIG.3.5 DAMAGE ACCUMULATION PLOTS (EACH SYMBOL REPRESENTS A SPECIMEN)

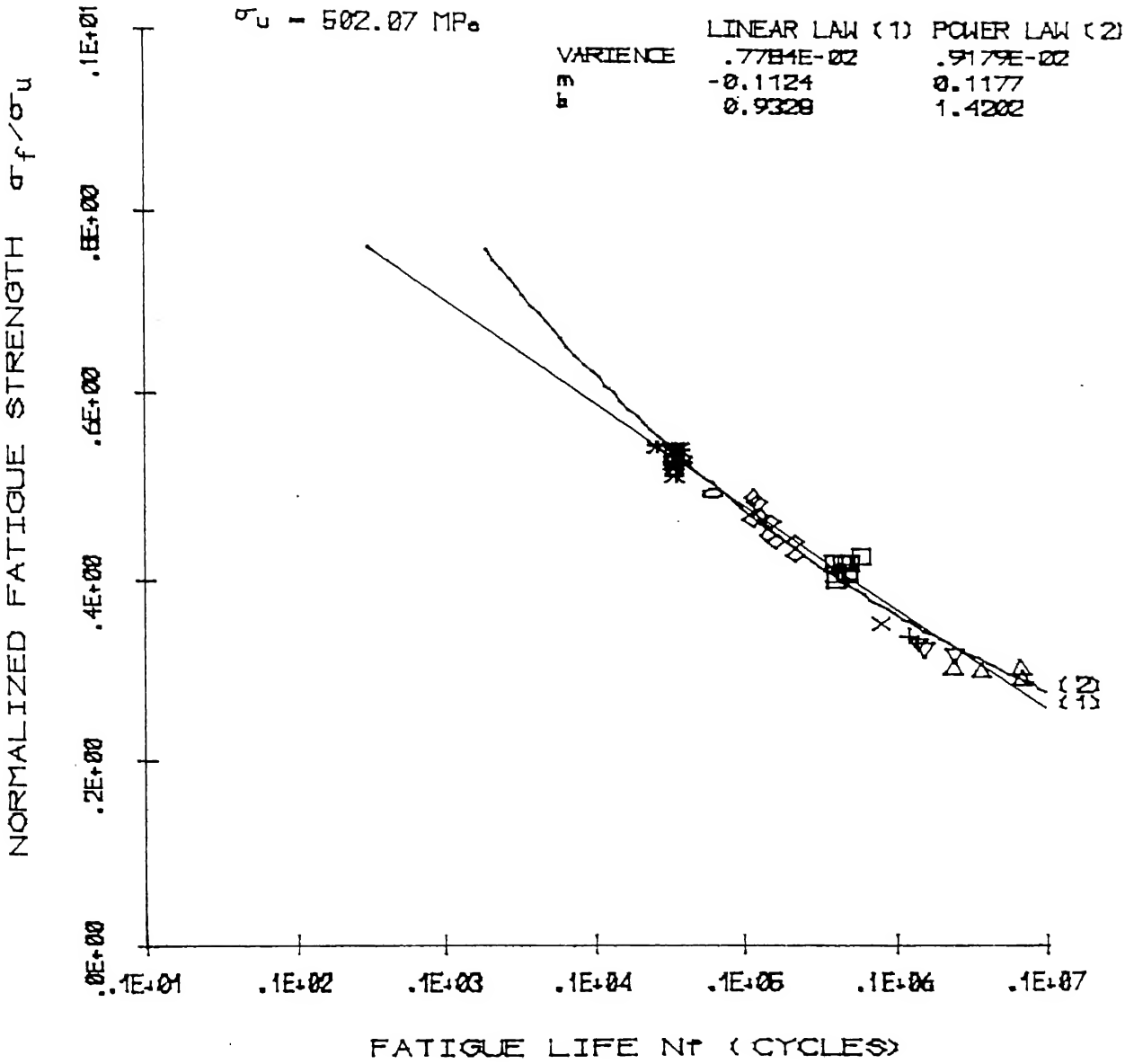

FIG.3.6 STRESS-FATIGUE LIFE CURVE

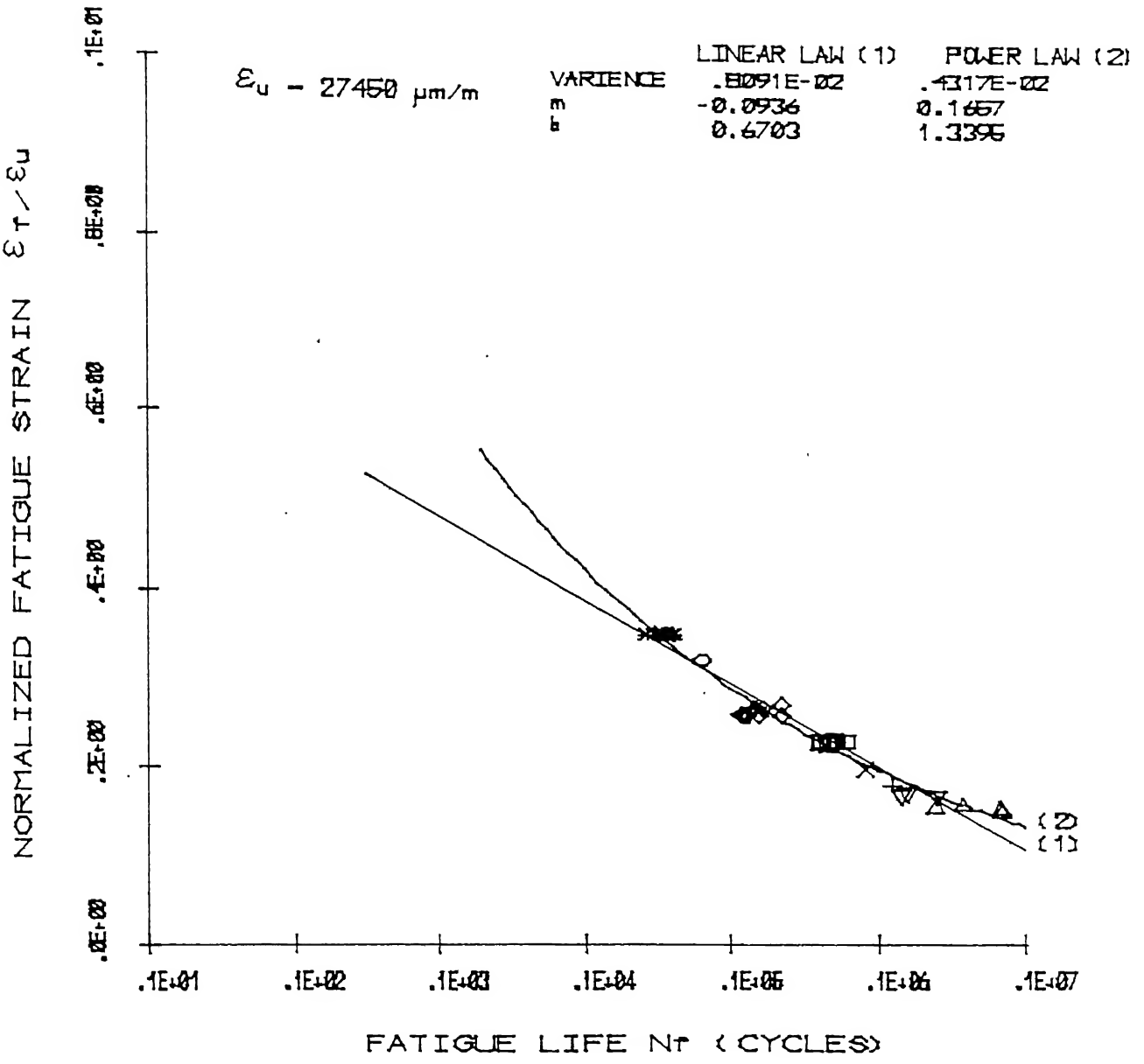

FIG.3.7 STRAIN-FATIGUE LIFE CURVE

The failure criterion and the fracturographic study of the specimen has been given in the next section. The development of the damage model and the analytical model for probability S-N curve have been described later in the next to next sections.

3.1 FRACTURE MECHANISM:

The failure criterion applied is an important consideration in the damage propagation plots (Figs. 3.2 - 3.5). Salkind [1] suggested that for composites, fatigue test data should be reported in terms of the change in stiffness for number of cycles rather than fracture. A small change in stiffness may define the failure in stiffness critical applications, such as springs whereas in load critical applications, such as tension cables, the load decay below a particular level or complete separation may be the failure. Many investigators [6,18-20] have used the separation as the criterion of failure. Whereas some others have used a particular loss in stiffness as the criterion of failure, namely 15 % by Kharan [17]. Sims and Brogdon [12] extended the Tsai-Hill failure criterion for static tests to fatigue tests. Hahn and Kim [11] first stated that failure occurs when the fatigue secant modulus reduces to within the range of the static secant modulus. O'Brien, et.al. [25] defined a secant modulus failure criterion based on the statement of Hahn and Kim [11]. The criterion may be stated as The failure occurs when fatigue secant modulus degrades from its initial tangent modulus to the static secant modulus. Hwang and Hahn [35] have given a strain failure criterion for the load controlled mode of loading, which is defined as - the failure in a material occurs when the fatigue resultant strain reaches the static ultimate strain.

For stroke controlled mode of loading secant modulus failure criterion is found most suitable and has been used as the failure criterion in the present studies. A schematic representation of this criterion (for the stroke controlled mode) on stress-strain axes is shown in Fig. 3.8.

Curve ABCD represents the static test stress-strain curve. AB is the elastic deformation and D is the fracture point. Thus the slope of line AB represents the elastic modulus or tangent modulus E_o and the slope of line AD represents the static secant modulus $E_{st.sec.}$ The stress and strain corresponding to fracture point, D, are ultimate tensile strength, σ_u, and ultimate strain, ε_u, respectively. In fatigue cycling for the first one-fourth cycle stress-strain curve ABC follows the same static stress-strain curve.

The first cycle is represented by ABCEFG. The slope of line AC represents the first cycle fatigue secant modulus. The stresses and strains at C and F are maximum and minimum in the cycle respectively. In further cycles the strain limits remains the same as the loading is stroke controlled, whereas the maximum stress continuously decreases with number of cycles. Thus the cycle PQRST for which maximum stress (Point T) falls on static secant modulus line AD (i.e. when fatigue secant modulus reduces to static secant modulus) is considered as cycle at failure. It can be observed from the same figure (Fig. 3.8) that the hysterisis loop is widest for first the cycle which goes on narrowing with number of cycles and ultimately become stable after few cycles.

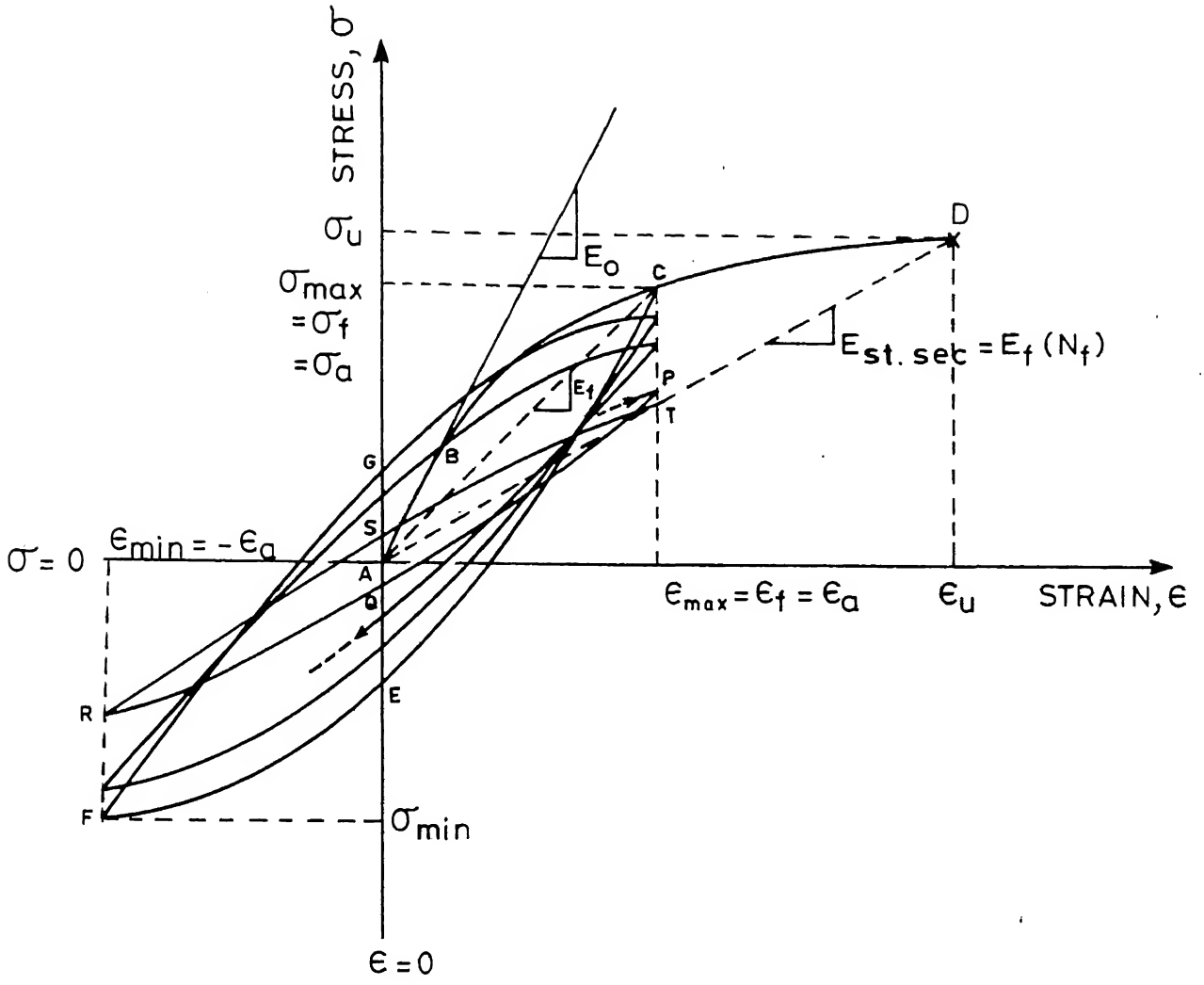

Fig. 3.8 Fatigue secant modulus failure criterion .

Table 3.1 shows that the fatigue secant modulus at first cycle is less than static tangent modulus, although the strain amplitude is within static proportional limit. It may be because of high strain rate in fatigue tests. The first cycle fatigue secant modulus is low for high strain amplitudes, because, for high strains, the material goes into plastic range in first cycle itself. Normalized damage has been calculated considering first cycle fatigue secant modulus therefore, the damage occurred in the first cycle is not considered in damage propagation plots (Figs. 322 to 3.5).

An examination of Figs. 3.2 to 3.5 shows that the normalized damage propagation is dependent on deflection or strain amplitude. The experimental points in the figures show that the damage propagation can be divided into three steps, namely the damage initiation step (Step I), steady damage step (Step II) and the damage propagation step (Step III).

All the three steps are clearly visible and can be distinguished for 18 and 21 mm displacements (Fig. 3.3 and 3.4 respectively). For lower displacements of 12 and 13 mm (Fig. 3.2) Step III is comparatively larger and Step II is smaller. For higher displacement of 26 mm (Fig. 3.5) Step I is comparatively larger and Step II is smaller. It is also clear from the figures that the damage during Step I is lower for lower displacements and higher for higher displacements. More exploration of figures reveals that the period of Step III is smaller for higher displacements and larger for lower displacement. That is the damage in last cycles is sudden for higher displacements and of a progressive nature

for lower displacements.

The initial damage (during Step I) can be analysed as follows. Bunsell [5] has shown that for Kevlar-49 fibers, the hysteresis loop is wide enough in the first few cycles which becomes narrower and stable after-ward. In these first few cycles 0.2% plastic strain deformation occurs. It was experienced during experiments too that the temperature increases in first few cycles and then stabilizes. Modulus of the fiber decreases with temperature increase (0.2 GPa/^{o}C approximately for the range of 25^{o} to 50^{o}C [46]). Thus firstly because of temperature increase and plastic deformation in first few cycles, fatigue secant modulus decreases i.e. damage increases. The temperature increase was larger for higher strain amplitudes, so the initial damage is larger for higher displacements. Secondly some voids are always present in composite which work as stress concentrators in the material. These stress concentrators may be relieved by cracking of highly localized stressed matrix within first few cycles after which damage rate becomes slow. Thirdly the initial damage may be due to individual fiber failures resulting from statistically distributed fiber strength. Initial damage may also be due to debonding in early cycles as described by Owen et.al. [6] for glass fiber composites. However, no surface damage was observed under microscopic examination in Step I.

It was observed that matrix cracks developed on the surface of specimen near the fixed end in steady damage step (Step II)

range. Microscopic examination shows that most of the cracks were at the crest of fiber strands. In some specimens the cracks are exactly at the fixed end in a straight transverse line, whereas in some other specimens it is scattered to a distance of 10 mm away from the fixed end as shown in photographs of Fig. 3.9. The reason for the difference may be the difference in grip pressure. There was only a slight reduction in modulus even after these matrix cracks had developed over full width of specimen. Because of this very small damage occuring in Step II it is termed steady damage step.

As the specimen enters into the damage propagation step (Step III) from steady damage step (Step II) a number of fracture events occur, as follows. The matrix cracks in resin phase and debonding around the transverse fiber strands have occured in early cycles of Step III which were propagated along longitudinal fiber strands in later cycles as shown in Fig. 3.10. The number of these cracks increased in the neighbourhood of fixed end with number of cycles and took the form of small delamination of size 5 - 10 mm, which results in a fast degradation of modulus. Determinations were confirmed by ultrasonic flaw detector. Extensive study by UVD may be carried out in future.

Moreover, it was observed under polarised light in a microscope that the fibers under the matrix-cracks on surface developed in Step II, were broken out and even some fiber ends came out from cracks, as shown in schematic Fig. 3.11(a).

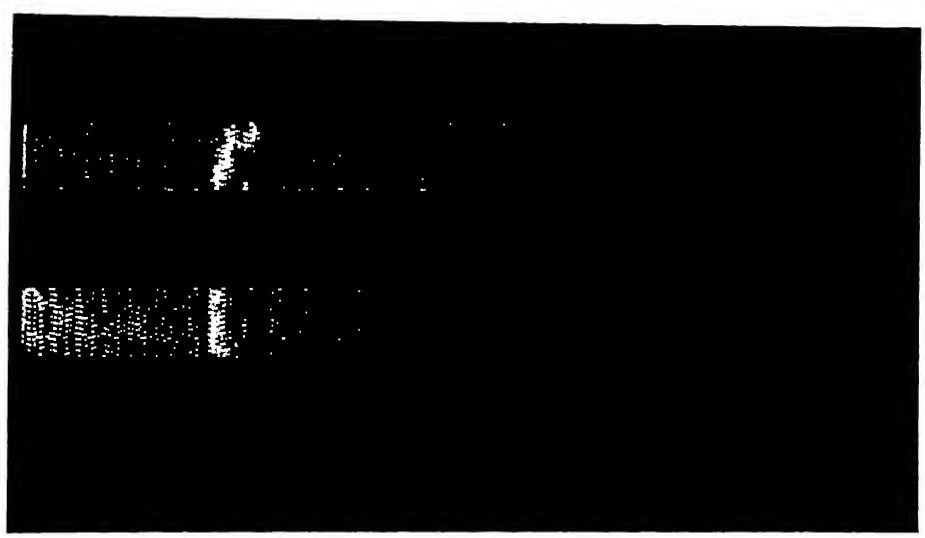

Fig. 3.9: Matrix crack on specimen surface (in straight line at fixed end and scattered near fixed end).

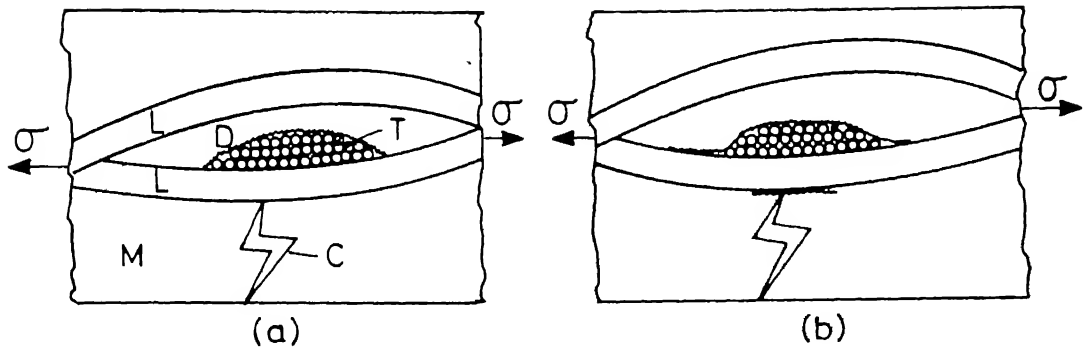

M - Matrix ; L - Longitudinal fiber; T - Transverse fiber;
C - Crack in matrix ; D - Debonding

Fig. 3.10 Schematic diagram of crack propogation in laminate (the sections are parallel to load direction)
(a) Matrix crack in matrix and debonding around transverse fiber strand
(b) Propogation of both cracks along longitudinal fiber.

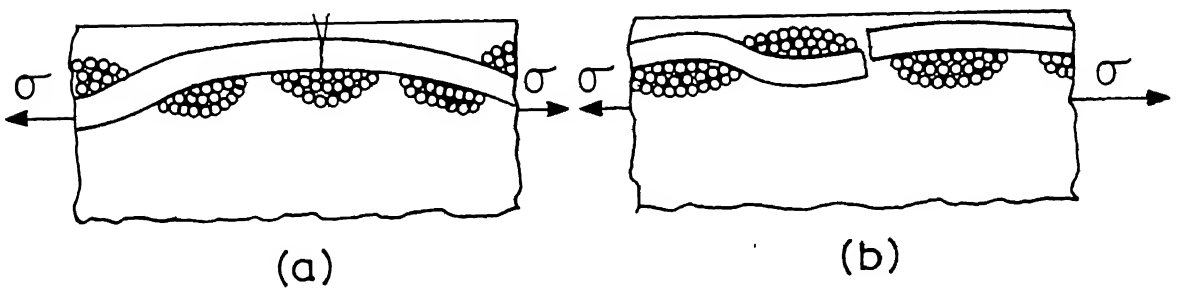

Fig. 3.11 Schematic diagram of fiber breaking in laminate (the sections are parallel to load direction)
(a) Fiber break at the crest of the fiber strand
(b) Breaking of fiber going under the transverse fiber strand.

It was seen that because of convolution of the fiber strands, the fiber strand going under the transverse fiber strand were broken at the bend and came upward and were seen at the level of transverse fibers, as shown in Fig. 3.11(b). The breaking of these few fiber stands includes the whole outer layer to break dramatically. The outer layer failure greatly reduces the modulus resulting in sudden damage which increases upto the final failure. The outer-layer break some times meets the delamination near the surface and then the delamination part is crushed in compression cycles. It was seen in the static tests that the yielding first took place in the compression side thus in fatigue it may be possible that the damage occurs, due to compression yielding and buckling of fibers.

3.2 DAMAGE MODEL DEVELOPMENT:

A number of investigators have studied the progressive nature of the damage in fatigue of composites. Some investigators [9, 18-21] studied it qualitatively whereas many others [7, 22,36-38] studied it quantitatively and developed the different damage models to predict damage accumulation during fatigue. Hwang and Han [38] have critically reviewed the available damage models. They have also proposed few new models.

In general fatigue damage of a material depends on number of a material depends on number of fatigue cycle, applied stress level, cyclic frequency, temperature, moisture content and geometry of the specimen, etc. The damage can be written in a functional form as,

$$D = F(N, \sigma_f, R, f, T, M, \ldots) \qquad (3.5)$$

where,

N : number of fatigue cycle,

σ_f : fatigue stress, i.e. σ_{max},

R : fatigue stress ratio, i.e. $\sigma_{max}/\sigma_{min}$,

f : cyclic frequency,

T : temperature,

M : moisture content,

σ_{max} : maximum stress in fatigue cycle,

σ_{min} : minimum stress in fatigue cycle.

As a first approach the effect of frequency and environmental conditions are neglected. The fatigue stress ratio, R can be taken as constant (= - 1) for the present study. Hence,

$$D = F(N, \sigma_f) \qquad (3.6)$$

As fatigue stress, σ_f, can be expressed in terms of fatigue life, N_f, with the help of S-N curve. The number of fatigue cycle, N, can be normalized by N_f to simplify the function, F. Thus damage, D, can be expressed as,

$$D = F(N_{nor}, \sigma_f) \qquad (3.7)$$

where,

$$N_{nor} = f(N, N_f)$$

The function, F, have been suggested by a number of investigators in different form. Out of which few have been tried for present damage accumulation and the Fong's equation [38,47] with some modification is found best applicable. Fong

$$D = \frac{e^{cN_{nor}} - 1}{e^{c} - 1}, \qquad c \neq 0$$

$$= N_{nor} \qquad c \neq 0 \qquad (3.10)$$

Equation 3.10 is a single variable equation. Simplicity of the equation is the reason for choosing the damage and the normalized number of cycles such that they vary from zero to one.

It was found that this model does not describe the initial damage occuring during fatigue. Thus it was necessary to add a term in model which takes initial damage into account. It was seen from damage accumulation plots (Fig. 3.2 - 3.5), that the initial damage had monotonically decreasing damage rate whereas rest of the damage had monotonically increasing damage rate. Thus an equation similar to Eq. 3.10 but replacing both damage, D, and normalized number of cycles, N_{nor}, by their conjugates, is added in Eq. 3.10 with some weighing constant. The final damage model will be,

$$D = A\left(\frac{e^{c_1 N_{nor}} - 1}{e^{c_1} - 1}\right) + (1 - A)\left(1 - \frac{e^{c_2(1-N_{nor})} - 1}{e^{c_2} - 1}\right) \qquad (3.11)$$

where,

c_1, c_2, A : constants.

The constants were found out by fitting the model to experimental points by minimizing variance through Powel's method.

The model is fitted for each fatigue stress separately and shown in Figs. 3.2 - 3.5 alongwith the experimental points. The nature of curves and values of constants c_1, c_2, and A in Fig. 3.2 - 3.5 clearly show that they depend on fatigue stress. Although, due to scarcity of data it is not possible to find out the definite relationship, the trend seems clear. The constant, c_1 which indicates the monotonically increasing damage rate, increases with increase in fatigue stress. As c_1 decreases, the damage propagation becomes more gradual, for low fatigue stress, damage propagates much gradually whereas it propagates suddenly in last few cycles for higher stresses. The constant, c_2, which indicates the monotonically decreasing damage rate, decreases with increase in fatigue stress. The constant A, which is the weighing function of monotonically increasing damage rate term, decreases with fatigue stress i.e. the initial damage is larger for higher stresses. It was also observed that this damage model indicates the damage accumulation quite well for middle range of fatigue stress (i.e. 18 and 21 mm displacements) whereas it deviates slightly from the experimental points for lower and higher fatigue stresses (i.e. 12 and 26 mm respectively).

3.3 PROBABILITY S-N CURVE:

The normalized fatigue strength and fatigue strain, as already defined have been plotted against fatigue life on a semi-log graph paper in Figs. 3.6 and 3.7 respectively. The nature of the curves is as expected i.e. fatigue life increases as fatigue stress or strain decreases.

In general fatigue to static strength ratio (i.e. normalized fatigue strength) can be expressed as follows,

$$\frac{\sigma_f}{\sigma_u} = F\,(N_f,\ R,\ f,\ T,\ \ldots\ ) \qquad (3.12)$$

where,

σ_f : fatigue strength,

σ_u : static strength,

N_f : fatigue life,

R : fatigue stress ratio,

f : cyclic frequency,

T : temperature.

The function F has to be evaluated experimentally. It is therefore, necessary to simplify the equation to make it applicable to design analysis too. For this purpose neglecting the effect of frequency, f, and temperature, T, and taking fatigue stress ratio, R, a constant (= -1) for present study, the Eq.3.12 reduces to,

$$\frac{\sigma_f}{\sigma_u} = F\,(N_f) \qquad (3.13)$$

The nature of the function, F, has been suggested by a number of investigators [7,8,10-12,35,36,47] to develop analytical model for S-N curve. However, it has been observed that the S-N curve of composite materials can often be represented by a linear law with fatigue life on log scale [7,8,11],

$$\frac{\sigma_f}{\sigma_u} = m \log_{10} N_f + b \qquad (3.14)$$

where,

m, b : constants.

Another useful relationship to represent fatigue data is a power law [10,11],

$$\left(\frac{\sigma_f}{\sigma_u}\right) N_f^m = b \qquad (3.15)$$

where again,

m, b : other constants.

Equations similar to Eq. 3.14 and 3.15 can be written for fatigue to static ultimate strain ratio as,

$$\frac{\varepsilon_f}{\varepsilon_u} = m \log_{10} N_f + b \qquad (3.16)$$

and, $$\left(\frac{\varepsilon_f}{\varepsilon_u}\right) N_f^m = b \qquad (3.17)$$

where,

ε_f : fatigue strain (i.e. maximum strain in fatigue cycle

ε_u : static ultimate strain.

In the Eq. 3.14 - 3.17, the constants m and b are not universal constants. Hence they are found experimentally. These equations are fitted in experimental data by regression analysis. The values of constants and the corresponding curve fitted are shown in Figs. 3.6 and 3.7. The curves fit quite well.

Examination of S-N curves reveals that the analytical models fail at static strength or very low cycle fatigue range (N_f < about 200 cycles) as it shows fatigue strength more than static strength. It can be explained for composites from the fatigues damage consideration which is more critical for low cycle fatigue [1]. Fatigue strength of composites is more sensitive to strain range and since damage in static tests is also progressive, the high fatigue stresses might produce that much damage in first cycle itself that it will result in final fracture within further few cycles [10]. Moreover, it should be noted that the strain rate was much higher for fatigue tests than static tests. One should expect higher values of the static strength at the higher strain rate [10] which would have the effect of making the S-N curve correct in low cycle fatigue range.

A much higher fatigue life at lower fatigue stress, as observed from S-N curve, can be due to the fact that these stresses remains in linear or elastic stress range. Thus a very few cracks develop in first cycle that may not be accumulated to failure for the fatigue stresses below a particular level. Thus below that fatigue stress the analytical model will again fail.

An important feature of Fig. 3.6 and 3.7 is the observed scatter of the life at a given stress or strain level. While the extent of scatter varies slightly from one stress level to another, it approximately amounts to about double of the value.

However, for glass fiber composites it was observed to about one order of magnitude by most of the investigators. The scatter data for Kevlar fiber composites are rarely available. Minar et.al. [3] shown a much large scatter for Kevlar and therefore, Lubin [46] has suggested that a large number of specimens should be tested. But the scatter found in present study is quite small, which also results in reduction of number of specimen tested at each stress level.

The reason of scatter as found by many investigators [14,15] are,

1. Highly anisotropic nature of the composites.
2. Batch-to-batch variation of resin, fiber and sizing.
3. Local variation of resin cure, resin content or fiber distribution, and fiber orientation within a piece.
4. Piece-to-piece variation due to resin flow, air bubbles, wrinkles, fiber joints.
5. Difference in environmental conditions as temperature (elevated temperature magnifies the scatter), and moisture content, etc.

For present study the possibility of batch-to-batch variation is eleminated by taking all the specimen at a stress level from one laminate. This may be one of the reason of small scatter, obtained.

The fatigue stresses and lives which are obtained by analytical models (Eqs. 3.14 - 3.17) are the best fit to the values contained in the scatter band of the test results. These

values are for a probability of survival of 50 percent, so that half of the population will survive and half will fail when subjected to a particular stress level. Since much higher probabilities of survival are generally needed to avoid failures in actual structures, a statistical analysis of the test results is conducted.

Different investigators have estimated the data scatter assuming different distributions, such as log normal [6,14] and Weibull [11,12,22-24,36,47] distributions. Most of the investigators found the two parameter Weibull distribution as the best distribution for the fatigue data analysis. The three parameter Weibull distribution has the difficulty of having negative position parameter i.e. possibility of getting negative fatigue life which is not possible. Thus present scatter in the life data is analysed by two parameter Weibull distribution,

$$P(x \leq X) = 1 - \exp\left[- \left(\frac{X}{\beta}\right)^{\alpha} \right] \qquad (3.18)$$

where,

P : unreliability or probability of failure at X i.e. the probability of a random variable, x, being less than a particular value, X,

α : shape parameter,

β : scale parameter.

It is observed that there are several ways of analyzing the data with the Weibull modal by selecting the random variable, x, in different ways [11,12,22,24,36,47]. One of the way, described

by Hahn and Kim [11] and supported by Sims et.al. [12], selected for the present analysis is as follows,

$$X = N_{f\ nor} = N_f / N_{f\ th} \tag{3.19}$$

where,

$N_{f\ nor}$: normalized fatigue life,

N_f : fatigue life,

$N_{f\ th}$: theoretical fatigue life predicted from one of the Eq. 3.14 - 3.17 for a particular stress or strain.

Thus Eq. 3.18 can be rewritten as,

$$P = 1 - \exp\left[- \left(\frac{N_{f\ nor}}{\beta} \right)^{\alpha} \right] \tag{3.20}$$

where,

P : probability of fatigue life being shorter than N_f at the particular stress or strain for which $N_{f\ th}$ is calculated.

From normalized fatigue life, $N_{f\ nor}$, the shape and scale parameters can be estimated by simple regression analysis. This technique requires an assignment of numerical values of P_i (called the rank) for each experimental point $N_{f\ nor\ i}$. There are many ways of making this assignment, but in this study the median rank method, as used By Chou et.al. [42], is used. Here the experimental points, $N_{f\ nor\ i}$, are ordered from lowest to highest and then experimental P_i is assigned by the approximate median rank formula,

$$P_i = \frac{i - 0.3}{n + 0.4}, \quad i = 1,2,\ldots, n \tag{3.21}$$

where,

n : total number of experimental points.

In using linear regression the Eq. 3.20 can be transformed, by taking the logarithm twice, into the form,

$$y = \alpha x - \alpha \ln \beta \tag{3.22}$$

where,

$$x = \ln N_{f\ nor} \tag{3.23}$$

$$y = \ln \ln \left(\frac{1}{1-p}\right) \tag{3.24}$$

For each experimental $N_{f\ nor\ i}$, the corresponding values of x_i's are evaluated by Eq. 3.23 and for each experimental rank value, P_i, experimental y_i's are evaluated from Eq. 3.24. The theoretical values of y_i's associated with the theoretical distribution (Eq. 3.20), is evaluated by Eq. 3.22 at each experimental x_i's. The difference $y_i - y_i'$, which represents the error, is squared and summed over i as,

$$\Delta^2 = \sum_{i=1}^{n} (y_i - y_i')^2$$

$$= \sum_{i=1}^{n} (y_i - \alpha x_i - \alpha \ln \beta)^2 \tag{3.25}$$

This sum of the square of errors is then minimized, by forming the two equations,

$$\partial \Delta^2 / \partial \alpha = 0 \tag{3.26}$$

and $$\partial \Delta^2 / \partial \beta = 0 \tag{3.27}$$

Solving these two equations yields the two unknown parameters as,

$$\alpha = \frac{\sum_{i=1}^{n} x_i y_i - \frac{1}{n} \sum_{i=1}^{n} x_i \sum_{i=1}^{n} y_i}{\sum_{i=1}^{n} x_i^2 - \frac{1}{n} \left(\sum_{i=1}^{n} x_i \right)^2} \tag{3.28}$$

$$\beta = \exp \left[\frac{\alpha \sum_{i=1}^{n} x_i - \sum_{i=1}^{n} y_i}{n \alpha} \right] \tag{3.29}$$

Although, the shape parameter, α, may change with the fatigue stress or strain, due to limited number of experimental points at each stress or strain level, α is assumed independent of fatigue stress or strain. The data at various stress or strain level can, then, be pooled to estimate single shape and scale parameters.

The experimental points N_f nor i's and P_i's are plotted in Fig. 3.12 along with the theoretical curve (Eq. 3.20) associated with fatigue stress power law (Eq. 3.14). The theoretical distribution curve is found to be fitted quite well, which assures the use of Weibull distribution. Similar curves associated with Eq. 3.15 - 3.17 can be drawn.

Commonly it is required to find out the fatigue life corresponding to some fatigue stress or strain with some probability of failure. It is, therefore, required to draw a P-S-N curve on normalized fatigue stress versus log of fatigue life

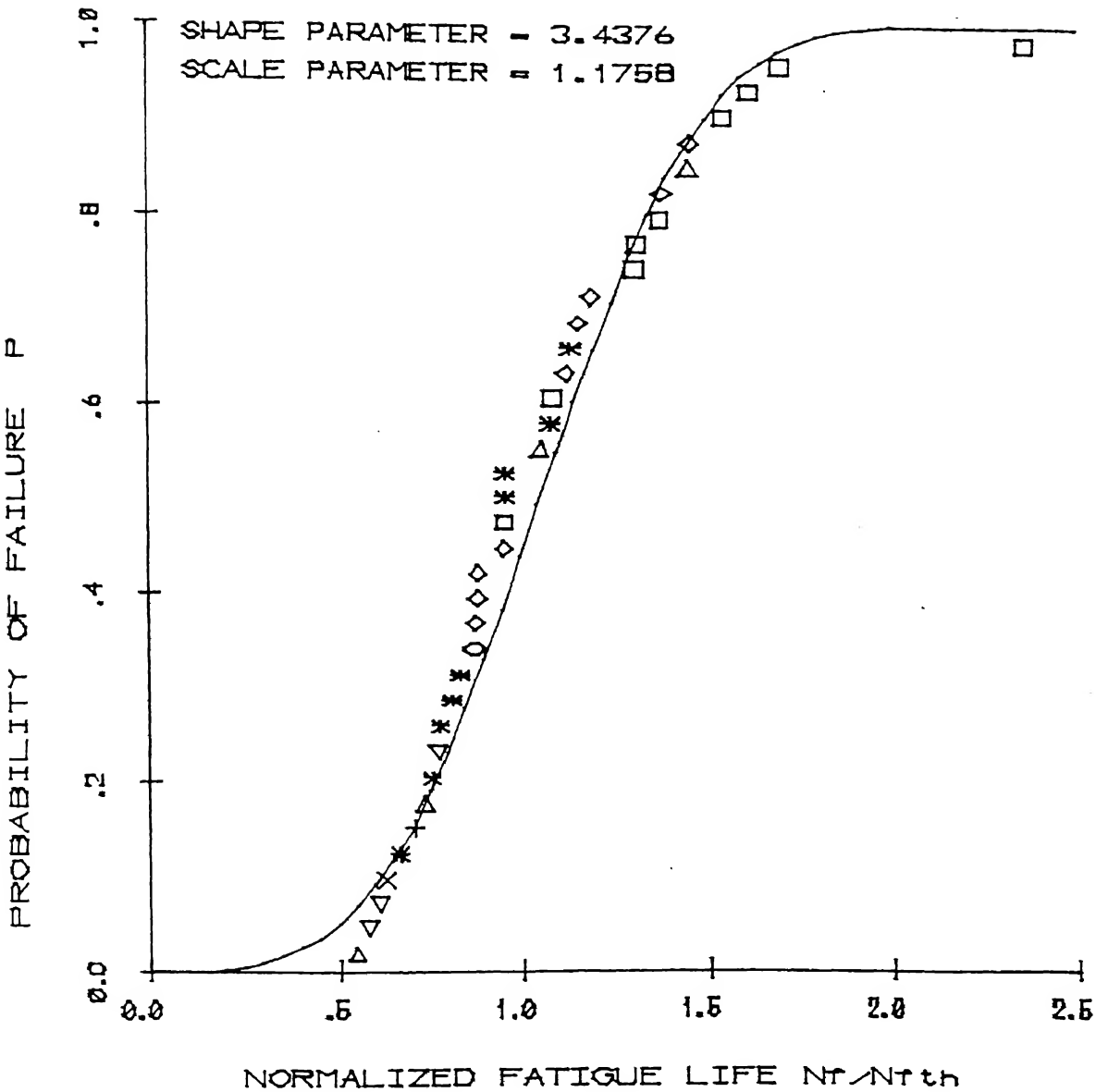

FIG.3.12 CUMULATIVE PROBABILITY DISTRIBUTION CURVE (SYMBOLS ARE SAME AS IN FIG.3.6)

coordinate keeping probability as parameter. A P-S-N curve for fatigue stress power law (Eq. 3.14) correlating Fig. 3.6 and 3.12 is drawn in Fig. 3.13, for the five probabilities of failure , namely 1, 10, 50, 90 and 99 percent.

3.4 CONCLUSIONS:

1. The Kevlar fiber composite laminates can be sectioned with the help of a fine toothed metal slitting H.S.S. cutter using slant side of teeth at high speed with plenty of water as coolant.

2. The accumulation of damage of Kevlar fabric reinforced epoxy composite in flexural fatigue can be divided into three steps, the damage initiation, steady damage, and the damage propagation. Although the damage accumulation depends on fatigue stress or strain, it follows a definite trend.

3. The damage accumulation can be predicted approximately by a damage model, consisting of two terms, a monotonically increasing damage rate term and the other decreasing damage rate as follows,

$$D = A\left(\frac{e^{c_1 N_{nor}} - 1}{e^{c_1} - 1}\right) + (1 - A)\left(1 - \frac{e^{c_2(1-N_{nor})} - 1}{e^{c_2} - 1}\right).$$

where,

D = normalized damage $(0 \leq D \leq 1)$

$$= \frac{E_f(1) - E_f(N)}{E_f(1) - E_f(N_f)}$$

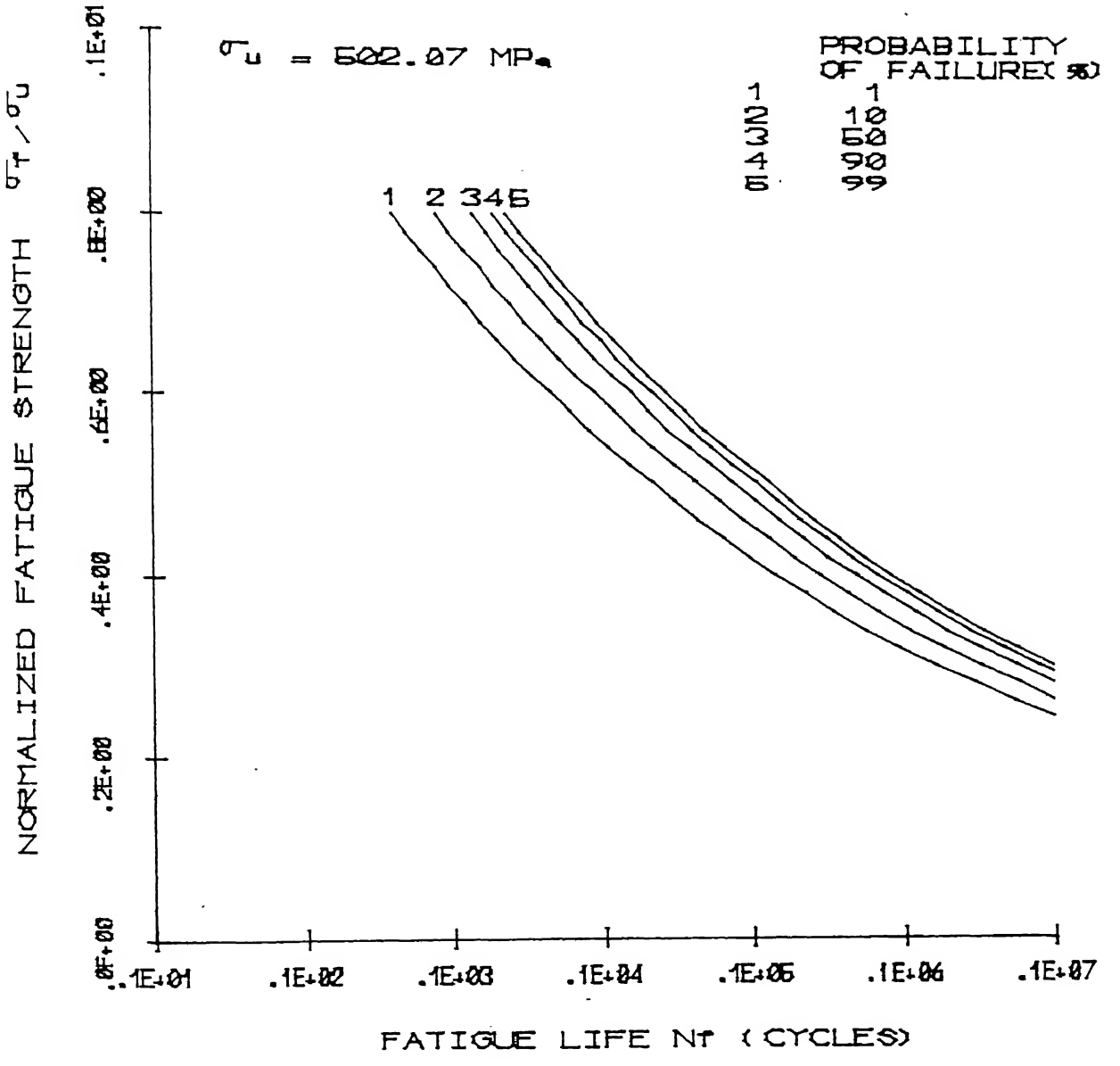

FIG.3.13 P-S-N CURVE

$E_f(N)$: fatigue secant modulus at N number of cycles,

N_f : fatigue life,

N_{nor} : normalized number of cycles $(0 \leq N_{nor} \leq 1)$
$= (N-1)/(N_f-1)$

c_1 : constant of monotonically increasing damage rate term,

c_2 : constant of monotonically decreasing damage rate term,

A : weighing constant.

The constants c_1, c_2 and A depend on fatigue stress or strain and have to be determined experimentally.

4. The S-N curve has been represented by a linear law between either of normalized fatigue stress or strain and logarithm of fatigue life. A slightly better representation has been obtained by power law between either of normalized fatigue stress or strain and fatigue life.

5. The scatter in fatigue life has been analysed by two parameter Weibull distribution and data at each stress level can be pooled by normalizing the fatigue life with theoretical fatigue life at the particular stress level predicted by analytical model for S-N curve. The S-N curves at different probability have been drawn with the help of following equation,

$$P = 1 - \exp\left[-\left(\frac{N_{f\,nor}}{\beta}\right)^{\alpha}\right]$$

where,

$N_{f\ nor}$: normalized fatigue life
= $N_f/N_{f\ th}$

N_f : fatigue life

$N_{f\ th}$: theoretical fatigue life predicted from analytical model of S-N curve for a particular stress or strain.

P : probability of fatigue life being shorter than N_f at the same stress or strain level at which $N_{f\ th}$ is calculated

α : shape parameter

β : scale parameter.

5.5 SCOPE OF FUTURE WORK:

1. Fracturographic study of more specimens could be done to find out the exact fracture mechanism of Kevlar fabric reinforced composites.

2. The flexural fatigue tests should be carried out with stress ratio, more than zero such that the fracture due to repeated tension and compression could be found out separately.

3. Experiments should be carried out at more displacement limits such that the relationship between the constants of damage model proposed and the applied fatigue stress or strain could be found out.

4. More damage models should be tried out such that the damage model could be applicable at every stress level with same confidence.

5. The effect of stress level on fatigue life data scatter distribution could be found out by testing more specimens at each stress levels.

REFERENCES

1. M.J. Salkind, Fatigue of Composites, Composite Materials: Testing and Design (Second Conference) ASTM-STP 497, p. 143-169, 1972.

2. B.D. Agarwal and L.J. Broutman, Analysis and Performance of Fiber Composites, A Wiley Interscience Publication, 198

3. L.H. Miner, R.A. Wolffe and C.Z. Zweben, Fatigue, creep, and impact resistance of aramid fiber reinforced composites Composite Reliability, ASTM STP 580, p. 549-59, 1975.

4. M.A. Hamstad and T.T. Chiao, Acoustic emission from stress rupture and fatigue of an organic fiber composite, ASTM-STP p. 201, 1975.

5. A.R. Bunsell, The tensile and fatigue behaviour of Kevlar- (PRD-49) fiber, J. Mat. Sci. V10, p. 1300, 1975.

6. M.J. Owen, T.R. Smith, and R. Dukes, Failure of glass-reinforced plastics, with special reference to fatigue, Plastics and Polymers, p. 227, June, 1969.

7. J.W. Dally and B.D. Agarwal, Low cycle fatigue behaviour of glass fiber reinforced plastics, Proceedings of the Army Symposium on Solid Mechanics, AMMRC-MS70-5, 1970.

8. B.D. Agarwal and J.W. Dally, Prediction of low-cycle fatig behaviour of GFRP: an experimental approach, J.Mat.Sci. V10 N1, p. 193-99, 1975.

9. T. Tanimoto and S. Amijima, Progressive nature of fatigue damage of glass fiber reinforced plastics, J. Comp. Mat. V9, p. 380, Oct. 1975.

10. C.K.H. Dharan, Fatigue failure mechanisms in a unidirection reinforced composite material, Fatigue of Composite Materia ASTM-STP 569, p. 171-188, 1975.

11. H.T. Hahn and R.Y. Kim, Fatigue behaviour of Composite laminate, J. Comp. Mat. V10, p. 156, April, 1976.

12. D.[illegible] Sims and V.H. Brogdon, Fatigue behaviour of composites under different loading modes, Fatigue of Filamentary Compo Materials, ASTM-STP 636, p. 185-205, 1977.

13. C.K.H. Dharan, The fatigue behavior of fiber-reinforced polymers and advanced composites, ASME, 1977.

14. H.C. Kim and L.J.Ebert, Fatigue life limiting parameters in fiberglass composites, J.Mat.Sci. V14, p. 2616, 1979.

15. T.K. James, F.J. Appl and C.W. Bert, Low cycle fatigue of a glass-fabric-reinforced plastic laminate, Experimental Mechanics, V8, p. 327.

16. L. Lessna, J. Levens, and J. Thompson, Flexural fatigue of glass reinforced thermoplastics, SPI, 24-th Annual Technical Conference, Washington, D.C., Section 1-C, Feb.19

17. C.K.H. Dharan, Fatigue failure mechanism in pultruded graphite polyester composites, Scientific Research Staff, Ford Motor Company, Tech. Report No.SR-74-71, June, 1974.

18. S.K. Juneja, Flexural fatigue studies on unidirectionally reinforced glass fiber epoxy composites, Ph.D. Thesis, IIT Kanpur, India, April, 1979.

19. B.D. Agarwal and S.K. Juneja, Flexural fatigue of a unidirectional composite in the longitudinal direction, Mat.Sci. and Engg. V46, p. 63, 1980.

20. B.D. Agarwal and S.K. Juneja, Strain-controlled flexural fatigue of unidirectional composites, Comp. Tech. Review, V4 N1, p. 6-13, Spring, 1982.

21. H.C. Kim and L.J. Ebert, Flexural fatigue behaviour of unidirectional fibreglass composites, Fiber Sci. and Tech. V14, p. 3, 1981.

22. J.N. Yang and D.L. Jones, Statistical fatigue of Graphite/Epoxy angle-ply laminates in shear, J. Comp.Mat. V12, p.371, Oct. 1978.

23. P.C. Chou and R. Cronan, Scale effect in fatigue of composite materials, J. Comp. Mat. V13, p. 178, July, 1979.

24. P.C. Chou and Robert Croman, Degradation and sudden death models of fatigue of graphite/epoxy composites, Composite Materials: Testing and Design (Fifth Conference), ASTM- STP p. 451-454, 1979.

25. T.K. O'Brien and K.L. Reifsnider, Fatigue damage evaluation through stiffness measurements in Boron-epoxy laminates, J. Comp. Mat.V15, p. 55, Jan. 1981.

26. H.C. Kim and L.J. Ebert, Axial fatigue sequence and mechani in unidirectional fiberglass composites, J.Comp.Mat.V20, p.139, April, 1978.

27. K.H. Boller, Fatigue characteristics of RP laminates subjected to axial loading, Mod. Plast. V41, p.145, 1964.

28. J.W. Davis, J.A. McCarthy, and J.N. Schurb, The fatigue resistance of reinforced plastics, Mater. Des.Eng. p.87-91, 1964.

29. S. Amijima and T. Tanimoto, The effect of glass content and environmental temperature on the fatigue properties of laminated glassfiber composite materials, Mech. Behaviour of Materials, Proceeding of the 1971 International Conference on Mechanical Behaviour of Material, Vol.V, The Society of Material Science, Japan, p. 269-78, 1972.

30. T. Tanimoto and S. Amijima, Fatigue properties of laminated glassfiber composite materials, SPI, 29th Annual Technical Conference, Washington, D.C., Section 17-B, Feb.1974.

31. B.E. Kaminski, Effects of specimen geometry on the strength of composite materials, Analysis of the Test Methods for High Modulus Fibers and Composites, ASTM-STP 521, p.181-91, 1973.

32. J.W. Dally and L.J. Broutman, Frequency effect on the fatigue of G.R.P., J. Comp. Mat. V1, p. 424, 1967.

33. C.C. Shih and L.J. Ebert, Flexural failure mechanisms and global stress plane for unidirectional composites subjected to four-point bending tests, Composites, V17, N4, p. 309, Oct. 1986.

34. T.M. Whitney, C.E. Browning and A. Mair, Analysis of the flexural test for laminated composite materials, Composite Materials: Testing and Design (Third Conference) ASTM-STP 54(p. 30-45, 1974.

35. W. Hwang and K.S. Han, Fatigue of composites Fatigue modules concept and life prediction, J. Comp. Mat. V20, p.154, March, 1986.

36. H.T. Hahn, Fatigue behavior and life prediction of composite laminates, Composite Materials: Testing and Design (Fifth Conference), ASTM-STP 674, p. 383-417, 1979.

37. A. Poursartip, M.F. Ashby, "Damage accumulation during fatigue of composites, Scripta Metallurgica, V16, p. 601, 1982.

38. W. Hwang and K.S. Han, Cumulative damage models and multi-stress fatigue life prediction, J. Comp. Mat. V20, p.125, March, 1986.

39. L.L. Clements, Problems in testing aramid/epoxy composites, Failure modes in composites IV, edited by J.A. Cornie and F.W. Crossman, p. 176-183, A Publication of the Metallurgical Society of AIME, 1979.

40. L.L. Clements and T.T. Chiao, Engineering design data for an organic fiber/epoxy composite, Composites, V8, p.87, 1977.

41. B. Jacob, V. Diwakar, S.Arumugham, T.S. Lakshmanan and B.K. Sarkar, Strength and failure mode correlation in Kevlar/epoxy composite, Fiber Sci. and Tech., V20, p.13-23, 1984.

42. C. Zweben, The flexural strength of aramid fiber composites, J. Comp. Mat. V12, p.422, Oct. 1978.

43. S. Fischer and G. Maron, A complete elastic-plastic analysis of aramid fiber composites, Fiber Sci. and Tech., V20, p. 91-98, 1984.

44. R.M. Jones, Apparent flexural modulus and strength of multimodulus materials, J. Comp.Mat. V10, p. 342, 1976.

45. M.M. Schwartz, Composite material hand-book, McGraw-Hill Book Company, 1984.

46. G. Lubin, Handbook of composites, Van Nostrand Reinhold Co., p. 273-312, 1982.

47. G.P. Sendeckyj, Fitting Models to Composite Material Fatigue Data, Test Methods and Design Allowables for Fibrous Composites, ASTM - STP 734, Ed. C.C. Chamis, pp. 245-60, 1981.